

Analysis of Mechanical Properties of Fiber-reinforced Composites
with Random Microstructure

by

Jan Zeman

Czech Technical University
Faculty of Civil Engineering

1999

Approved by_____

(Chairperson of Supervisory Committee)

Program Authorized

to Offer Degree_____

Date_____

TABLE OF CONTENTS

List of Figures	iv
List of Tables	vi
List of Algorithms	viii
Chapter 1: Introduction and historical review	1
1.1 Concept of a representative volume element	2
1.2 Description of microstructure morphology	3
1.3 Genetic algorithms and simulated annealing method	4
1.4 Effective properties of composite materials	6
1.5 Present work	7
1.6 Notation	8
Chapter 2: Quantification of microstructure morphology	9
2.1 Basic concepts and hypotheses	9
2.1.1 Concept on an ensemble	10
2.1.2 Ergodic hypothesis	11
2.1.3 Statistical homogeneity	11
2.1.4 Statistical isotropy	12
2.2 Microstructure description	12
2.2.1 Microstructure description for general composites	12
2.2.2 Microstructure description for particulate composites	15

2.2.3	Relating S and ρ functions for particulate microstructures	18
2.3	Determination of microstructural statistics for real materials	20
2.3.1	Functions S_n	21
2.3.2	Functions ρ_n	22
2.3.3	Microstructural statistics for some theoretical models of microstructures	23
2.4	Analysis of real microstructure	26
2.4.1	Testing ergodic hypothesis	27
2.4.2	Test of statistical isotropy	29
2.4.3	Microstructure describing functions	30
2.4.4	Conclusions	32
Chapter 3:	Construction of the periodic unit cell	33
3.1	Objective function and problem definition	34
3.2	Deterministic algorithms	38
3.2.1	Powell's method (POWELL)	40
3.2.2	Dynamic Hill Climbing (DHC)	40
3.2.3	BFGS method	40
3.2.4	Test example	40
3.3	Stochastic optimization methods	42
3.3.1	Principle of genetic algorithm	43
3.3.2	Sampling mechanisms	44
3.3.3	Genetic operators	46
3.3.4	Genetic algorithm I (GA I)	49
3.3.5	Genetic algorithm II (GA II)	50
3.3.6	Genetic algorithm III (GA III)	51
3.3.7	Hybrid genetic algorithm (HGA)	51
3.3.8	Differential evolution (DE)	52

3.3.9	Augmented simulated annealing (AUSA)	53
3.3.10	Test example	54
3.4	Some additional improvements	56
3.4.1	Adaptive operator probabilities	56
3.4.2	Problem-dependent operators	58
3.4.3	Sampling grid refinement	62
3.5	Determination of periodic unit cell	62
Chapter 4:	Effective properties of periodic composite medium	68
4.1	Basic relations	68
4.1.1	Hill's lemma	70
4.1.2	Stress and strain concentration factors	70
4.2	Mori-Tanaka method	71
4.3	Finite element formulation	72
4.4	Numerical results	74
Chapter 5:	Conclusions and future work	78
	Bibliography	80
	Appendix A: Evaluation of $M(r)$ for impenetrable cylinders	87
	Appendix B: Parameter settings for optimization algorithms	89

LIST OF FIGURES

1.1	A real micrograph of a transverse plane section of the graphite fiber tow . . .	1
1.2	Principle of simulated annealing method	5
2.1	Example of sampling template	21
2.2	Correction factor	22
2.3	Unit cell for hexagonal lattice of fibers	24
2.4	Function $K(r)$ for hexagonal packing of fibers	25
2.5	Microstructural functions for fully penetrable cylinders.	26
2.6	Idealized binary image of a transverse cross-section of a fiber tow	27
2.7	Selected members of the sample space	28
2.8	Two-point matrix probability function $S_{mm}(\mathbf{x} - \mathbf{x}')$ and variation coefficient $v(\phi)$ of $S_{mm}(r, \phi)$ plotted as a function of r/R	29
2.9	Two-point matrix probability $S_{mm}(r)$ and unique relations for the general two-point probability function $S_{rs}(r)$	30
2.10	Second order intensity function $K(r)$ and radial distribution function $g_2(r)$.	31
2.11	The two-point matrix probability function	32
3.1	Geometry of the periodic unit cell	34
3.2	An admissible unit cell	41
3.3	Allowable position of particle	60
3.4	Periodic unit cells with corresponding second order intensity functions	63
3.5	Variation of the objective function with the number of particles in the PUC.	64
3.6	Evolution of the 10 particles PUC	65

3.7	Periodic unit cells: (a) Hexagonal lattice, (b) 2-fibers PUC, (c) 5-fibers PUC, (d) 10-fibers PUC.	66
4.1	Example of Finite Element meshes: (a) Hexagonal lattice, (b) 2-fibers PUC, (c) 5-fibers PUC, (d) 10-fibers PUC.	75

LIST OF TABLES

2.1	Relation of two-point probability functions	15
3.1	Minimum values of function	42
3.2	Number of function evaluations for deterministic optimizers	43
3.3	Characteristics of the best individual	55
3.4	Number of function evaluations for stochastic optimizers	56
3.5	Initial operator probabilities resulting from adaptation procedure	58
3.6	AUSA algorithm with adaptive operator probabilities	58
3.7	AUSA algorithm with problem-dependent operators	62
4.1	Material properties of T30/Epoxy system	74
4.2	Components of the effective stiffness matrix	76
4.3	Variation of effective stiffness tensor for five ten-particle PUC resulting from optimization	76
4.4	Variation of effective stiffness tensor for five randomly picked ten-particle PUC	77
B.1	Deterministic algorithms parameters	89
B.2	Parameter settings for GA I	89
B.3	Parameter settings for GA II	90
B.4	Parameter settings for HGA	90
B.5	Parameter settings for GA III	91
B.6	Parameter settings for DE	91
B.7	Parameter settings for AUSA	92

B.8	Adaptivity parameters setting	92
B.9	Parameter settings for AUSA with problem-dependent operators	93

LIST OF ALGORITHMS

3.1	Golden Section search	37
3.2	Principle of deterministic optimizations	39
3.3	The <i>Distant-point</i> algorithm	39
3.4	Principle of genetic algorithm	44
3.5	Augmented Simulated Annealing	67

ACKNOWLEDGMENTS

I would like to express my deepest gratitude and thanks to my advisors, Ing. Miroslav Černý, CSc. and especially to Ing. Michal Šejnoha, Ph.D for their support, endless patience, continuous encouragement and inspiration during the whole course of this work. In addition, I would like to thank Prof. Ing. Jiří Šejnoha, DrSc. for his numerous valuable suggestions and inspiring ideas.

I extend my appreciation to Ing. Karel Matouš and Mr. Matěj Lepš for the fruitful discussions and useful guesses from the field of the evolutionary computation.

Jan Zeman

Prague

December 1999

Czech Technical University
Faculty of Civil Engineering

Abstract

Analysis of Mechanical Properties of Fiber-reinforced Composites with Random Microstructure

by Jan Zeman

Effective elastic properties of the graphite-epoxy unidirectional fiber composite with fibers randomly distributed within the transverse plane section are found. To enhance the efficiency of numerical analysis the complicated real microstructure is replaced by a material representative volume element consisting of a small number of particles, which statistically resembles the real microstructure.

First, various statistical descriptors suitable for the microstructure characterization of a random media are considered. Several methods for the determination of these descriptors are proposed and tested for some simple theoretical models of microstructures. Moreover, a validity of various statistical hypotheses usually accepted for a random heterogenous media is checked for the present material as well.

Successively, the unit cell is derived from the optimization procedure formulated in terms of these statistical descriptors. A variety of deterministic as well as stochastic optimization algorithms is examined to solve this problem. It is shown that for this particular application stochastic method based on genetic algorithm combined with the simulated annealing method is superior to other approaches.

Finally, the estimates of elastic properties are found for the resultant unit cells using the Finite Element Method. Results suggest that the proposed approach, which effectively

exploits the knowledge of material's statistics of the composite, is more reliable than various averaging techniques or simple unit cell models based on the regular fiber distribution.

Chapter 1

INTRODUCTION AND HISTORICAL REVIEW

The elastic as well as the inelastic behavior of composite materials is strongly dependent on the geometrical arrangement of distinct phases of the composite – *microstructure*. On the contrary, conventional methods for the prediction of thermo-mechanical response of composite materials are either based on limited microstructural information such as volume fraction of phases (see eg. [Gibson, 1994]) or deal with a regular distribution of phases (see eg. [Aboudi, 1991, Teplý and Dvořák, 1988]).

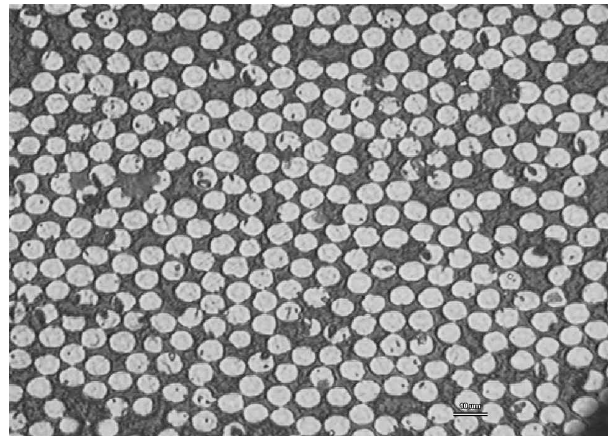


Figure 1.1: A real micrograph of a transverse plane section of the graphite fiber tow

Unfortunately, microstructure of real composite materials is typically quite complicated. To illustrate this fact, we present a high-contrast micrograph of a part of the graphite fiber tow impregnated by the polymer matrix, Fig. 1.1. Evidently, such a composite can hardly be characterized by a simple periodic unit cell commonly used for the rectangular and hexagonal

arrangement of fibers. The characterization of microstructure by the volume fractions of fiber or matrix only do not captures evident clustering of fibers. On the other hand it appears possible to select such a micrograph directly as a objective of analysis. However, once we realize, that this particular sample contains approximately 300 particles it becomes clear that the resulting analysis will be extremely difficult, especially in the inelastic regime. To tackle this problem, one can substitute the whole complex microstructure by its *representative volume element* (RVE) and perform the analysis on the RVE instead on the whole sample.

1.1 Concept of a representative volume element

The crucial question now is how to determine such a volume element. In his classical work [Hill, 1963], Hill states that:

This phrase (representative volume) will be used when referring to a sample that (a) is structurally entirely typical of the whole mixture on average, and (b) contains sufficient number of inclusions for the apparent overall moduli to be effectively independent of the surface values of traction and displacement, so long as these values are ‘macroscopically uniform’.

The above conditions imply that the RVE should contain a large number of inhomogeneities to include all possible configurations appearing in the composite. This leads to a general, quite vague, suggestion that the RVE should be “sufficiently large” compared to the typical size of the inhomogeneity.

Another perhaps more rigorous approach proposed by [Povirk, 1995] relies on the description of the original microstructure by a certain statistical function and then requires the RVE to approximate the original function as good as possible. In order to provide “sufficient” number of particles and meet the aforementioned conditions, *periodicity* of such a RVE is often considered – we presume that the RVE is surrounded by the periodic replicas of itself. This procedure enables us to substitute complicated original microstructure by the *periodic*

unit cell which consists of a small number of reinforcement only but still carries non-trivial statistical informations and is capable of capturing the real response of composite material. This approach is used in this work.

1.2 Description of microstructure morphology

A literature offers a number of statistical descriptors of a random composite media. The most suitable for the present purpose are the *n-point probability function* S_n defined in [Torquato and Stell, 1982], which gives the probability of simultaneously finding n points in the matrix or fiber phase and the *generic n-particle probability density* ρ_n [Boublík, 1996, Quintanilla and Torquato, 1997], which gives the probability density for finding particle centers in given n points. Unfortunately, obtaining these descriptors for values of n higher than two for real materials is prohibitively difficult, so the higher-order correlation functions are of little practical importance.

Pioneering work devoted to determination of S_n -type functions for micrographs of real media is attributed to [Corson, 1974]. Despite the fact that the proposed procedure was extremely cumbersome (it was based on manual evaluation of photographs taken from samples of the real material) the principle itself (evaluation of the S_n function on some sampling grid and then averaging of the corresponding values) was used and extended in following works. In [Berryman, 1984] Corson's procedure was automated by the use of image processing technique and finally, [Smith and Torquato, 1988] proposed simple simulation method for the determination of functions S_n , which is suitable for non-digitized media as well.

The approach for obtaining ρ_n -type function used in this work is based on the *second order intensity function* $K(r)$ defined by [Ripley, 1977], which can be easily determined for particulate microstructure. Unlike the preceding method this procedure is not simulation-based and therefore $K(r)$ can be evaluated very rapidly for a reasonable number of reinforcements.

1.3 Genetic algorithms and simulated annealing method

Genetic algorithms (GAs) are adaptive methods which may be used to solve general search and optimization problems. The basic idea behind these methods are the genetic processes of biological organisms – namely the evolution and self-organization of natural systems over many generation according to the principle of natural selection and “survival of the fittest”. In reality, individuals of one population compete with each other for natural resources and for attracting a mate. Those which succeed in obtaining resources and attracting mates will have large number of offsprings, while individuals performing poorly will produce lesser number of descendants. So the abilities of successful individuals are more likely to be passed to following generations and result in the best adaption to the environment. GAs closely mimic all these natural processes – they work with a *population* of individuals, each represents a solution to a given problem. A *score* or *fitness* is assigned to each individual depending on how good solution it presents. The individuals with higher fitness are more likely to reproduce by *crossover* and to pass their characteristics to their offsprings. Moreover, an individual can also undergo a *mutation* if appropriate. In this way, over a number of successive population, the good characteristic of individuals are mixed and spread over all population, so the population converges to the optimal solution.

The earliest work on this subject was in fact Darwin’s *Origin of species* where aforementioned principles were stated. The basic principles of GAs were first rigorously laid down by [Holland, 1975], their detailed discussion is given eg. in [Beasley et al., 1993a, Goldberg, 1989, Michalewicz, 1992]. In their classical formulation, GAs work with the binary representation of objective variables. Michalewicz in [Michalewicz, 1992] proposed the GAs, which use the floating-point representation of search variables and showed their superiority for the real-valued function optimization.

The *Simulated annealing* (SA) method is based on physical rather than biological principles – the algorithm effectively exploits the analogy between optimization problem and the annealing process of solid bodies. In the physical process of annealing the temperature of

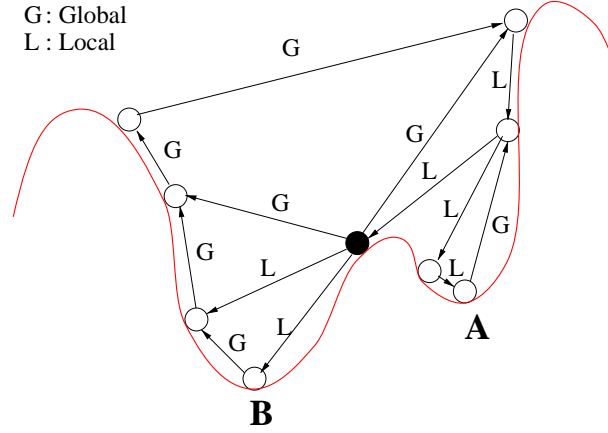


Figure 1.2: Principle of simulated annealing method

a solid is kept rather high initially and then decreases sufficiently slowly, so the individual particles have the possibility to attain the state with the minimal energy for a given constant temperature. As the temperature gradually decreases the energy of the whole body decreases as well and finally reaches the minimal value. SA algorithm works on the same principle - initial solution is generated randomly, some artificial parameter called *temperature* is set to initial value and new solutions are randomly generated. If the new solution is better than preceding in terms of fitness, it is accepted automatically and replaces the original solution. However, if the new solution is worse than the preceding one, it has still the chance to replace the original solution – this probability depends on the difference of objective function and actual temperature – which enables the solution to escape from local minimum (see Fig. 1.2). This procedure is repeated a number of times for constant temperature and then the temperature is decreased until it reaches certain prescribed minimal value. This version of algorithm was first proposed by [Kirkpatrick et al., 1983] and independently by [Cerny, 1985]. Detailed discussion of basic principles and further aspects of simulated annealing method can be found eg. in [Ingber, 1993, Ingber, 1995, Kvasnička, 1999].

In [Mahfoud and Goldberg, 1992] the efficient combination of GAs and SA methods was proposed. It exploits the essentials of GAs (a population of chromosomes, rather than one

point in space is optimized) together with the basic concept guiding the search towards minimal energy states. Some additional suggestions and methods for implementation are given in [Kvasnička, 1993].

1.4 Effective properties of composite materials

Pioneering work devoted to the problem of determination of effective properties of composite media is attributed to [Voight, 1887] and [Reuss, 1929]. However, most of the essential discoveries over the last decades are based on the famous Eshelby's finding [Eshelby, 1957] that the stress field in a ellipsoidal inclusion subjected to a uniform remote stress field is also uniform. This results allows to estimate the stress and strain fields in composite aggregate in terms of the phase elastic properties and certain stress and strain concentration tensors. These quantities can be generally derived either by employing a rigorous bounding procedures or by using some approximation techniques.

The first approach of the determination of elastic properties uses well known energy principles of elasticity to obtain bounds on effective elastic properties. The most noticeable contributors are [Hashin and Shtrikman, 1963, Beran, 1968, Milton, 1982] to name but a few.

A variety of approximation methods were proposed in the past 40 years. The most common procedures include dilute approximation, self-consistent method [Hill, 1965] and the Mori-Tanaka method [Mori and Tanaka, 1973, Benveniste, 1987]. In particular, the Mori-Tanaka method seems to be the most popular one due to it's simplicity and explicit estimates of the overall elastic moduli of composites.

When periodic media are under the consideration, it is possible to determine the local fields with the aid of a certain numerical method such as the *Finite Element Method*. However some constraints must be imposed on the objective fields in this case to take into account the periodicity of the media (see eg. [Teplý and Dvořák, 1988, Suquet, 1987] and the overview

[Michel et al., 1999]). However, once the local fields are known the procedure of the determination of effective properties is quite simple and straightforward.

1.5 Present work

The main objective of the present work is to apply previously introduced principles to analysis of the unidirectional fiber composite with carbon fibers embedded in polymer matrix - it means *two-phase material* generated by identical fibers of *circular cross section* whose generators are parallel. Morphology of such a material can be uniquely determined by its cross-section only so that the examined medium can be considered as a *two-dimensional* for statistical description as well as for proceeding numerical analysis.

Chapter 2 presents basic statistical descriptors for the two-phase media. First, the concept of an ensemble is briefly discussed and the principle of *ensemble averaging* is outlined. Successively, various hypotheses commonly applied to random composite materials are presented and discussed. Microstructural descriptors suitable for the characterization of the two-phase two-dimensional media are presented and methods for their determination for given materials are discussed and tested for some elementary theoretical configurations of particles. Finally, testing of some properties of statistical descriptors as well as their determination for the material displayed in Fig. 1.1 are performed.

Chapter 3 outlines determination of the RVE with the help of a certain minimization problem. A variety of deterministic and stochastic optimization algorithms is presented and their performance for the given problem is examined.

Chapter 4 briefly describes the evaluation of effective properties for a heterogeneous material. Finite Element Method is employed here to calculate the volume averages of local fields, which provide effective elastic properties of resulting composite media. The quality of unit cells resulting from optimization is compared with the results for the hexagonal array of fibers and with unit cells selected as a random cut of real microstructure.

1.6 Notation

Standard tensor and vector/matrix notation is used throughout the thesis. Tensor quantities are denoted either by lightface Greek letters eg. σ_{ij}, L_{ijkl} ; (3×1) and (6×1) vectors are denoted by lower-case boldface italic letters eg. $\boldsymbol{\sigma}$, (6×6) and (3×3) matrices are denoted by upper boldface Roman letters eg. \mathbf{L} and scalars are denoted by lightface eg. r .

The inverse of non-singular matrix is denoted by \mathbf{L}^{-1} and \mathbf{L}^T stands for transpose of matrix \mathbf{L} . Standard contracted notation is adopted when appropriate, thus $1 \equiv 11$, $2 \equiv 22$, $3 \equiv 33$, $4 \equiv 23$, $5 \equiv 13$ and $6 \equiv 12$.

Chapter 2

QUANTIFICATION OF MICROSTRUCTURE MORPHOLOGY

This Chapter provides introduction to basic principles and methods of statistical description of the random two-phase composite material. Initially, two basic approaches to microstructure description are outlined, for each case the microstructure of a random media is described by some general n -order statistical moments. Then, functions which incorporate statistical informations up to the two-point level are examined in more details. Despite the limitedness of such a description, these functions still carry sufficient amount of statistical informations to provide efficient tool for fulfilling the objective of this work - the RVE definition.

Section 2.1 explores basic concepts and hypotheses for the microstructure description of random composites. Section 2.2 introduces microstructural functions used in this work; their evaluation for different types of microstructure is presented in Section 2.3. Moreover, the connection between different approaches to the microstructure classification is examined and proposed methods are tested for some simple models of microstructures. Finally, these principles are in Section 2.4 applied to the analysis of micrographs taken from the real material.

2.1 Basic concepts and hypotheses

Consider again the micrograph displayed in Fig 1.1. In this particular case, arrangement of phases is exactly known (to a level of the microscope resolution) and one may assume that it completely describes the morphology of the whole composite. Unfortunately, when micrographs are taken from other parts of the specimen, microstructure of each sample is

substantially different (see Fig. 2.7). At this point, situation becomes quite complicated - the questions is, which of these micrographs is the most suitable for the foregoing analysis. To answer this question, one has to recognize the *random nature* of geometrical arrangements of phases - it means that the particular microstructure of a given sample yields only one possible arrangement of phases. Therefore, instead of determining the exact value of some quantity at a given point (which depends on actual sample), attention has to be turned to its *expected* or *averaged* or *macroscopic* value, which incorporates informations from all samples taken from a material.

2.1.1 Concept on an ensemble

To reflect the random character of the media under the consideration it is convenient to introduce the concept of an *ensemble* – the collection of a large number of systems which are different in their microscopical details but they are entirely identical within a point of view of macroscopic details (see eg. [Beran, 1968, Boublík, 1996]). Within this concept, *effective* or *expected* value of some quantity corresponds to the process of its averaging through all systems, forming the ensemble.

To formalize this idea, let us introduce a sample space \mathcal{U} , identify individual members of this space by α and define $p(\alpha)$ as the probability density of α in \mathcal{U} ([Drugan and Willis, 1996, Kohler and Papanicalou, 1982]). Then *ensemble average* of function $F(\mathbf{x}, \alpha)$ at point \mathbf{x} is provided by

$$\overline{F(\mathbf{x})} = \int_{\mathcal{U}} F(\mathbf{x}, \alpha) p(\alpha) d\alpha. \quad (2.1)$$

In the context of the quantification of microstructure morphology, ensemble represents the collection of material micrographs taken from different samples of the material. To follow the above definitions literary, experimental determination of the ensemble average of function $F(\mathbf{x}, \alpha)$ for a given point \mathbf{x} leads to the cumbersome procedure of manufacturing a large number of samples (which form the ensemble space \mathcal{U}), measuring $F(\mathbf{x}, \alpha)$ for every sample and then its averaging for all samples. So it appears to be meaningful to introduce

some hypotheses about the ensemble average, which substantially simplify this task.

2.1.2 Ergodic hypothesis

This hypothesis demands all states available to an ensemble of the systems to be available to every member of the system in the ensemble as well ([Beran, 1968]). Once this hypothesis is adopted, *spatial* or *volume average* of function $F(\mathbf{x}, \alpha)$ given by

$$\langle F(\mathbf{x}, \alpha) \rangle = \lim_{V \rightarrow \infty} \frac{1}{V} \int_V F(\mathbf{x} + \mathbf{y}, \alpha) d\mathbf{y} \quad (2.2)$$

is independent of α and identical to the *ensemble average*,

$$\langle F(\mathbf{x}) \rangle = \overline{F(\mathbf{x})}. \quad (2.3)$$

This hypothesis allows to examine only one arbitrary member of the sample space, provided that the sample is “sufficiently large” (see Eq. (2.2)). One possible way how to fulfill this condition is to assume periodic composite with a unit cell Ω . Then,

$$\lim_{V \rightarrow \infty} \frac{1}{V} \int_V F(\mathbf{x} + \mathbf{y}, \alpha) d\mathbf{y} = \frac{1}{\Omega} \int_{\Omega} F(\mathbf{x} + \mathbf{y}, \alpha) d\mathbf{y} \quad (2.4)$$

so for the ergodic periodic composite medium, the ensemble average is equal to the volume average taken over the unit cell.

2.1.3 Statistical homogeneity

Let us consider the situation when function F depends on n vectors $\mathbf{x}_1, \dots, \mathbf{x}_n$ rather than one vector \mathbf{x} . Then, *statistical homogeneity* assumptions means that value of the ensemble average is independent of the position of coordinate system origin [Beran, 1968, Torquato and Stell, 1982], so the expression

$$\overline{F(\mathbf{x}_1, \dots, \mathbf{x}_n)} = \overline{F(\mathbf{x}_1 - \mathbf{y}, \dots, \mathbf{x}_n - \mathbf{y})} \quad (2.5)$$

holds for an arbitrary value of \mathbf{y} . The most common choice is to set $\mathbf{y} = \mathbf{x}_1$, so

$$\overline{F(\mathbf{x}_1, \dots, \mathbf{x}_n)} = \overline{F(\mathbf{0}, \mathbf{x}_2 - \mathbf{x}_1, \dots, \mathbf{x}_n - \mathbf{x}_1)} = \overline{F(\mathbf{x}_{12}, \dots, \mathbf{x}_{1n})}, \quad (2.6)$$

where $\mathbf{x}_{ij} = \mathbf{x}_j - \mathbf{x}_i$. Therefore, if statistical homogeneity condition holds, ensemble average of F is a function of $n - 1$ variables only. Note that for periodic media this condition is satisfied automatically.

2.1.4 Statistical isotropy

When making the *statistical isotropy* assumption, we further extend the statistical homogeneity hypothesis. In this case, the ensemble average is not only independent on the position of the coordinate system origin but on the coordinate system's rotation as well. Under this hypothesis, the ensemble average depends on the absolute value of vectors $\mathbf{x}_{12}, \dots, \mathbf{x}_{1n}$ only:

$$\overline{F(\mathbf{x}_{12}, \dots, \mathbf{x}_{1n})} = \overline{F(r_{12}, \dots, r_{1n})}, \quad (2.7)$$

where $r_{ij} = \|\mathbf{x}_{ij}\|$.

2.2 Microstructure description

This Section presents basic statistical functions suitable for description of the microstructure of a random media. Although two different approaches to the microstructure characterization are employed here, in both cases statistical descriptors are obtained by similar procedure – initially, some fundamental random function relevant to the microstructure configuration is presented and then statistical moments of this function are identified as descriptors of microstructure morphology. Properties of the first and second order moments are thoroughly discussed in the sequel. Finally, connection between these two approaches is demonstrated.

2.2.1 Microstructure description for general composites

Fundamental function and statistical moments. The stepping stone of a general description of a random composite media is the introduction of the random stochastic function – *characteristic* or *indicator* function $\chi_r(\mathbf{x}, \alpha)$, which is equal to one when point \mathbf{x} lies in phase

r in the sample α and equal to zero otherwise [Beran, 1968, Torquato and Stell, 1982],

$$\chi_r(\mathbf{x}, \alpha) = \begin{cases} 1 & \mathbf{x} \in D_r(\alpha) \\ 0 & \text{otherwise.} \end{cases} \quad (2.8)$$

The symbol $D_r(\alpha)$ denotes here the domain occupied by r -th phase, r is further assumed to take values m for the matrix phase and f for the fiber phase respectively. Characteristic functions $\chi_f(\mathbf{x}, \alpha)$ and $\chi_m(\mathbf{x}, \alpha)$ are related, since the point \mathbf{x} must be located either in the matrix or in the fiber phase,

$$\chi_m(\mathbf{x}, \alpha) + \chi_f(\mathbf{x}, \alpha) = 1. \quad (2.9)$$

With the aid of this function, *general n -point probability* function S_{r_1, \dots, r_n} can be found using the ensemble average of the product of characteristic functions [Torquato and Stell, 1982, Beran, 1968, Drugan and Willis, 1996],

$$S_{r_1, \dots, r_n}(\mathbf{x}_1, \dots, \mathbf{x}_n) = \overline{\chi_{r_1}(\mathbf{x}_1, \alpha) \cdots \chi_{r_n}(\mathbf{x}_n, \alpha)}. \quad (2.10)$$

Thus, S_{r_1, \dots, r_n} gives the probability of finding n points $\mathbf{x}_1, \dots, \mathbf{x}_n$ randomly thrown into media located in the phases r_1, \dots, r_n .

Functions of the first and second order. Hereafter, we limit our attention to functions of the order of one and two, since higher-order functions are quite difficult to determine in practice. Therefore, description of the random media will be provided by the *one-point probability* function $S_r(\mathbf{x})$

$$S_r(\mathbf{x}) = \overline{\chi_r(\mathbf{x}, \alpha)}, \quad (2.11)$$

which simply gives the probability of finding the phase r at \mathbf{x} and by the *two-point probability* function $S_{rs}(\mathbf{x}, \mathbf{x}')$

$$S_{rs}(\mathbf{x}, \mathbf{x}') = \overline{\chi_r(\mathbf{x}, \alpha) \chi_s(\mathbf{x}', \alpha)}, \quad (2.12)$$

which denotes the probability of finding simultaneously phase r at \mathbf{x} and phase s at point \mathbf{x}' .

Moreover, these functions can be further simplified employing assumptions of statistical isotropy, homogeneity and ergodicity, as presented in Section 2.1. In particular for *statistically homogeneous* media we have

$$S_r(\mathbf{x}) = S_r, \quad (2.13)$$

$$S_{rs}(\mathbf{x}, \mathbf{x}') = S_{rs}(\mathbf{x} - \mathbf{x}'). \quad (2.14)$$

Suppose further that the medium is *statistically isotropic*. Then $S_{rs}(\mathbf{x} - \mathbf{x}')$ reduces to

$$S_{rs}(\mathbf{x} - \mathbf{x}') = S_{rs}(\|\mathbf{x} - \mathbf{x}'\|). \quad (2.15)$$

The ergodicity assumption makes possible to substitute the one-point correlation function of the statistically homogeneous media by its volume average ie. *volume concentration* or *volume fraction* of the r -th phase c_r ,

$$S_r = c_r. \quad (2.16)$$

Limiting values. In addition, the two-point probability function S_{rs} depends on the one-point probability function S_r for certain values of its arguments such that

$$\text{for } \mathbf{x} \rightarrow \mathbf{x}' : S_{rs}(\mathbf{x}, \mathbf{x}') = \delta_{rs} S_r(\mathbf{x}), \quad (2.17)$$

$$\text{for } \|\mathbf{x} - \mathbf{x}'\| \rightarrow \infty : \lim_{\|\mathbf{x} - \mathbf{x}'\| \rightarrow \infty} S_{rs}(\mathbf{x}, \mathbf{x}') = S_r(\mathbf{x}) S_s(\mathbf{x}'), \quad (2.18)$$

where symbol δ_{rs} stands for Kronecker's delta. Relation (2.17) states that probability of finding two different phases at one point is equal to 0 (see also Eq. (2.9)) or is given by the one-point probability function if phases are identical. Equation (2.18) manifests that for large distances points \mathbf{x} and \mathbf{x}' are statistically independent. This relation is often denoted as the *no-long range orders* hypothesis (see eg. [Willis, 1977]).

Finally, according to Eq. (2.9) we may determine one and two-point probability functions for all phases provided that these functions are given for one arbitrary phase. For one-point probability function of statistically homogeneous and ergodic media, this relation assumes trivial form:

$$c_m = 1 - c_f. \quad (2.19)$$

Relations for two-point probability functions of statistically isotropic and ergodic medium are summarized in Table 2.1. Note that symbol r which stands for $\|\mathbf{x}\|$ in Table 2.1 should not be mistaken with subscripted r used as a phase index heretofore.

<i>Known function</i>			
	$S_{mm}(r)$	$S_{mf}(r)$	$S_{ff}(r)$
$S_{mm}(r)$	$S_{mm}(r)$	$c_m - S_{mf}(r)$	$c_m - c_f + S_{ff}(r)$
$S_{mf}(r)$	$c_m - S_{mm}(r)$	$S_{mf}(r)$	$c_f - S_{ff}(r)$
$S_{ff}(r)$	$c_f - c_m + S_{mm}(r)$	$c_f - S_{mf}(r)$	$S_{ff}(r)$

Table 2.1: Relation of two-point probability functions

2.2.2 Microstructure description for particulate composites

Another approach to the microstructure characterization can be adopted when the composite material is *particulate* - it consists of particles with identical specific shape (eg. ellipsoids, cylinders etc.) embedded in a matrix phase. Microstructure morphology of such a composite can be described using only *centers* of particles. This approach is frequently used in the statistical mechanics of liquids (see eg. [Boublík, 1996, Chapter 6]). Its principles will be applied here.

Fundamental function and statistical moments. To be more specific, suppose that each sample α in \mathcal{U} is formed by N distinguishable particles with centers located at distinct points $\mathbf{x}_\alpha^1, \dots, \mathbf{x}_\alpha^N$ placed in a matrix of volume (area) V . Such a system of random points can be described by the random field density function $\psi(\mathbf{x}, \alpha)$ (see [Markov, 1998, Ponte Casteñada and Willis, 1995] and references herein)

$$\psi(\mathbf{x}, \alpha) = \sum_{i=1}^N \delta(\mathbf{x} - \mathbf{x}_\alpha^i), \quad (2.20)$$

where $\delta(\cdot)$ stands for Dirac's function.

Foregoing procedure is similar as in the Section 2.2.1. The *generic n-particle probability density function*¹ $\rho_n(\mathbf{x}_1, \dots, \mathbf{x}_n)$ ([Boublík, 1996, Quintanilla and Torquato, 1997]) for *distinct* points $\mathbf{x}_1, \dots, \mathbf{x}_n$ is found by ensemble averaging the product of basic functions,

$$\rho_n(\mathbf{x}_1, \dots, \mathbf{x}_n) = \overline{\psi(\mathbf{x}_1, \alpha) \cdots \psi(\mathbf{x}_n, \alpha)}, \quad (2.21)$$

which gives the probability density of finding a particle center in all points $\mathbf{x}_1, \dots, \mathbf{x}_n$ randomly thrown into the material.

Functions of the first and second order. As in the previous Subsection, we turn our attention to one and two-particle functions only. Thus, description of a material will be carried out by *generic one-particle probability density function*

$$\rho_1(\mathbf{x}) = \overline{\psi(\mathbf{x}, \alpha)}, \quad (2.22)$$

which gives the probability density for finding an inclusion centered at \mathbf{x} , and by *generic two-particle probability density function* provided by

$$\delta(\mathbf{x} - \mathbf{x}')\rho_1(\mathbf{x}) + \rho_2(\mathbf{x}, \mathbf{x}') = \overline{\psi(\mathbf{x}, \alpha)\psi(\mathbf{x}', \alpha)}, \quad (2.23)$$

which denotes the probability density of finding one inclusion centered at \mathbf{x} and the second one in \mathbf{x}' . The first term in Eq. (2.23) is added to take into account the situation, when points \mathbf{x} and \mathbf{x}' coincide (see also discussion bellow).

Again, under the assumption of statistical isotropy, homogeneity and ergodicity these functions simplify substantially. Hence, for *statistically homogeneous* media

$$\rho_1(\mathbf{x}) = \rho_1 \quad (2.24)$$

$$\rho_2(\mathbf{x}, \mathbf{x}') = \rho_2(\mathbf{x} - \mathbf{x}'). \quad (2.25)$$

¹ The generic *n*-particle probability density function can be derived via *specific n-particle probability density function* [Boublík, 1996, Quintanilla and Torquato, 1997]. However, this procedure is purely formal and of no practical use, so is omitted here.

Furthermore, if the material is *statistically isotropic* the $\rho_2(\mathbf{x} - \mathbf{x}')$ reduces to

$$\rho_2(\mathbf{x} - \mathbf{x}') = \rho_2(\|\mathbf{x} - \mathbf{x}'\|). \quad (2.26)$$

To this end, assuming the ergodicity of the media, one may equal the value of the one-point correlation function of statistically homogeneous media to the *number of particle centers per unit volume*,

$$\rho_1 = \rho = \lim_{V \rightarrow \infty} \frac{N}{V}. \quad (2.27)$$

Limiting values. For this approach it is meaningless to investigate the situation $\mathbf{x} \rightarrow \mathbf{x}'$ for the function $\rho_2(\mathbf{x}, \mathbf{x}')$, since one point \mathbf{x} cannot be occupied by two centers of distinguishable particles. However, recall that $\overline{\psi(\mathbf{x}, \alpha)\psi(\mathbf{x}', \alpha)}$ gives the probability density of finding particle centers located at points \mathbf{x} and \mathbf{x}' randomly thrown into sample. When points \mathbf{x} and \mathbf{x}' coincide, this probability density is simply equal to the probability density of finding a particle center at point \mathbf{x} . Therefore,

$$\text{for } \mathbf{x} \rightarrow \mathbf{x}' : \overline{\psi(\mathbf{x}, \alpha)\psi(\mathbf{x}', \alpha)} = \overline{\psi(\mathbf{x}, \alpha)} = \rho_1(\mathbf{x}). \quad (2.28)$$

Fortunately, the two-particle probability density function $\rho_2(\mathbf{x}, \mathbf{x}')$ for statistically homogeneous medium attains under the no-long range hypothesis similar form as the two-point probability functions

$$\text{for } \|\mathbf{x} - \mathbf{x}'\| \rightarrow \infty : \lim_{\|\mathbf{x} - \mathbf{x}'\| \rightarrow \infty} \rho_2(\mathbf{x}, \mathbf{x}') = \rho_1(\mathbf{x})\rho_1(\mathbf{x}'). \quad (2.29)$$

Since for the statistically isotropic and ergodic medium $\rho_1(\mathbf{x})\rho_1(\mathbf{x}') = \rho^2$ it is convenient to normalize this function to one for large distances of points \mathbf{x} and \mathbf{x}' . This requirement yields the definition of the *radial* or *pair distribution function* $g_2(\mathbf{x} - \mathbf{x}')$ [Axelsen, 1995, Boublík, 1996, Pyrz, 1994]

$$g_2(\mathbf{x} - \mathbf{x}') = \frac{\rho_2(\mathbf{x} - \mathbf{x}')}{\rho^2}. \quad (2.30)$$

Sometimes it is useful to describe the media by function, which is equal to zero rather than to one for large distances of points \mathbf{x} and \mathbf{x}' . The *total correlation function* $h(\mathbf{x} - \mathbf{x}')$

[Boublík, 1996] given by

$$h(\mathbf{x} - \mathbf{x}') = g_2(\mathbf{x} - \mathbf{x}') - 1 \quad (2.31)$$

is an example of such a function.

The definition of function ρ_n as a probability density results in its complicated determination for given microstructures. To overcome this problem, for statistically isotropic and ergodic media [Ripley, 1977] defined the *second order intensity function* $K(r)$ which gives the number of further points expected to lie within a radial distance r of an arbitrary point divided by the number of particles (fibers) per the unit area. This function is related to the radial distribution function by

$$g_2(r) = \frac{1}{2\pi r} \frac{dK(r)}{dr}. \quad (2.32)$$

At the end, let us briefly discuss the situation, when composite media under consideration are formed by non-overlapping particles. This condition implies that $\rho_2(\mathbf{x}, \mathbf{x}')$ is equal to zero for $(\mathbf{x} - \mathbf{x}') \in \Omega_d$; it means that some “secure area” Ω_d cannot be occupied by another particle center. For example, if we consider the unidirectional fiber composite with identical circular fibers of radius R , Ω_d is cylinder with center at point \mathbf{x} and radius $2R$.

2.2.3 Relating S and ρ functions for particulate microstructures

As noted before, the description of a media by functions ρ_n is suitable for material systems consisting of particles with specific shape, while the definition of functions S_n needs no such a type of initial assumption. The obvious question is how to relate this two types of approaches. To answer this question, it is necessary to establish the connection between characteristic function of one phase $\chi_r(\mathbf{x}, \alpha)$ and probability density function $\psi(\mathbf{x}, \alpha)$. It is easy to notice, that for the composite formed by impenetrable particles, this relation holds [Ponte Castañeda and Willis, 1995]:

$$\chi_f(\mathbf{x}, \alpha) = \int \psi(\mathbf{y}, \alpha) m(\mathbf{x} - \mathbf{y}) d\mathbf{y}, \quad (2.33)$$

where $m(\mathbf{y})$ is the characteristic function of one inclusion with center at the origin of coordinate system.

Performing ensemble averaging and using Eq. (2.23), one gives

$$\begin{aligned} S_{ff}(\mathbf{x}_1, \mathbf{x}_2) &= \int \int m(\mathbf{x}_1 - \mathbf{x}_3) m(\mathbf{x}_2 - \mathbf{x}_4) \left[\int \psi(\mathbf{x}_3, \alpha) \psi(\mathbf{x}_4, \alpha) p(\alpha) d\alpha \right] d\mathbf{x}_3 d\mathbf{x}_4 \\ &= \int \int m(\mathbf{x}_1 - \mathbf{x}_3) m(\mathbf{x}_2 - \mathbf{x}_4) [\delta(\mathbf{x}_3 - \mathbf{x}_4) \rho_1(\mathbf{x}_3) + \rho_2(\mathbf{x}_3, \mathbf{x}_4)] d\mathbf{x}_3 d\mathbf{x}_4. \end{aligned}$$

Considering statistically homogeneous ergodic media and using total correlation function $h(\mathbf{x}_3, \mathbf{x}_4)$ rather than $\rho_2(\mathbf{x}_3, \mathbf{x}_4)$, we arrive at expression

$$\begin{aligned} S_{ff}(\mathbf{x}_1 - \mathbf{x}_2) &= \rho \Omega_{int}(\mathbf{x}_1 - \mathbf{x}_2) + \rho^2 \Omega^2 + \\ &+ \rho^2 \int \int h(\mathbf{x}_3 - \mathbf{x}_4) m(\mathbf{x}_1 - \mathbf{x}_3) m(\mathbf{x}_2 - \mathbf{x}_4) d\mathbf{x}_3 d\mathbf{x}_4, \end{aligned} \quad (2.34)$$

where $\Omega_{int}(\mathbf{x}_1 - \mathbf{x}_2)$ stands for the intersection volume (area) of two particles with centers located at points \mathbf{x}_1 and \mathbf{x}_2 and Ω is the volume (area) of one particle. Once the S_{ff} function is known, one may obtain all the remaining functions with the help of relations summarized in Table 2.1. For example, the two-point matrix-matrix probability function is after some elementary manipulation provided by

$$\begin{aligned} S_{mm}(\mathbf{x}_1 - \mathbf{x}_2) &= 1 - \rho \Omega_u(\mathbf{x}_1 - \mathbf{x}_2) + \rho^2 \Omega^2 + \\ &+ \rho^2 \int \int h(\mathbf{x}_3 - \mathbf{x}_4) m(\mathbf{x}_1 - \mathbf{x}_3) m(\mathbf{x}_2 - \mathbf{x}_3) d\mathbf{x}_3 d\mathbf{x}_4, \end{aligned} \quad (2.35)$$

where $\Omega_u(\mathbf{x}_1 - \mathbf{x}_2) = 2\Omega - \Omega_{int}(\mathbf{x}_1 - \mathbf{x}_2)$ is the union volume (area) of two particles with centers located at points \mathbf{x}_1 and \mathbf{x}_2 . This relation is equivalent to formulas obtained by Torquato in [Torquato and Stell, 1985] using slightly different procedure.

To make Eq. (2.35) as simple as possible, let us consider statistically isotropic two-dimensional composite formed by identical circles with radius R . For this particular case, Eq. (2.35) yields

$$S_{mm}(r_{12}) = 1 - \rho \Omega_u(r_{12}) + \rho^2 \Omega^2 + \rho^2 \int \int h(r_{34}) m(r_{13}) m(r_{23}) d\mathbf{x}_3 d\mathbf{x}_4, \quad (2.36)$$

where Ω equals to πR^2 . Further, functions $m(\mathbf{x})$ and $\Omega_u(\mathbf{x})$ depend on $r = \|\mathbf{x}\|$ only and are given by

$$m(r) = \begin{cases} 1 & r \leq R \\ 0 & \text{otherwise} \end{cases}, \quad (2.37)$$

$$\Omega_u(r) = \begin{cases} 2R^2 \left[\pi - \arccos(r/2R) + r/2R \sqrt{1 - (r/2R)^2} \right] & r < 2R \\ 2\pi R^2 & r \geq 2R \end{cases}. \quad (2.38)$$

Thus, the only unknown term in Eq. (2.35) now is the integral

$$M(r_{12}) = \iint h(r_{34})m(r_{13})m(r_{24})d\mathbf{r}_3d\mathbf{r}_4. \quad (2.39)$$

Evaluation of this expression becomes simple once we realize that $M(r)$ is a double convolution. In such a case the Fourier transform of M is given as a multiplication of Fourier transforms of individual functions (see eg. [Rektorys, 1995a, Chapter 28])

$$\widehat{M}(t) = \widehat{h}(t)\widehat{m}(t)\widehat{m}(t). \quad (2.40)$$

After some manipulations, which are outlined in Appendix A, we arrive at

$$\widehat{m}(t) = \frac{2\pi R}{t} J_1(Rt) \quad (2.41)$$

$$\widehat{h}(t) = 2\pi \int_0^\infty h(r) J_0(rt) r dr = t \int_0^\infty \widetilde{K}(r) J_1(rt) dr, \quad (2.42)$$

where $J_0(\cdot)$ and $J_1(\cdot)$ in above equations are the Bessel functions of the first kind, zero and first order, respectively and $\widetilde{K}(r) = K(r) - \pi r^2$ is a counterpart of function $h(r)$.

Finally, the inverse Fourier transform can be then written as

$$M(r) = \frac{1}{2\pi} \int_0^\infty \widehat{M}(t) J_0(rt) t dt. \quad (2.43)$$

2.3 Determination of microstructural statistics for real materials

This Section exploits individual methods suitable for the determination of microstructure descriptors defined in the previous Section. For the n -point probability functions a simple simulation technique is proposed, while the determination of radial distribution function is performed by deterministic procedure. Finally, precision of these methods is tested for simple two-dimensional models of microstructure.

For all procedures, medium is supposed to be formed by N identical circles with radius R and centers located at positions $\mathbf{x}^1, \dots, \mathbf{x}^N$ embedded in the rectangle with dimensions $\langle 0; H_1 \rangle \times \langle 0; H_2 \rangle$. Furthermore, periodicity of the media is assumed.

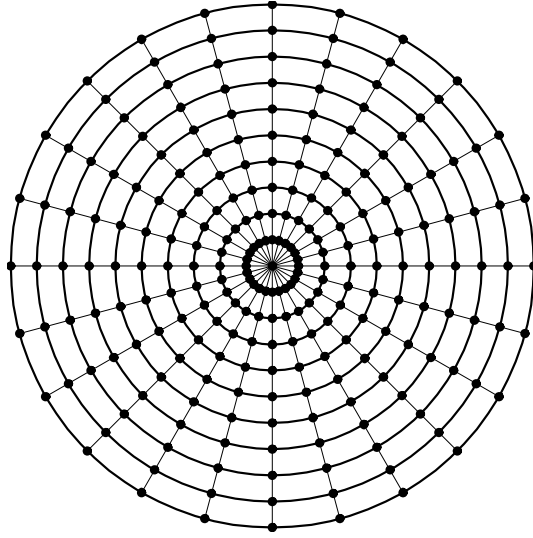


Figure 2.1: Example of sampling template

2.3.1 Functions S_n

The procedure of S_n functions determination is based directly on their definition - recall that for statistically homogeneous media eg. function S_m gives the chance of finding the randomly placed point located in the matrix phase. To determine this quantity, simple Monte-Carlo like simulation can be performed - we throw randomly point in the microstructure and count successful “hits“ into the matrix phase. Then, the value of function S_m can be estimated as

$$S_m \approx \frac{n'}{n}, \quad (2.44)$$

where n' is the number of successful hits and n denotes the total number of throws. Similar procedure can be used to determine values of $S_{mm}(\mathbf{x})$.

In [Smith and Torquato, 1988] faster procedure for the determination of function $S_{mm}(\mathbf{x})$ was proposed. Instead of tossing a line corresponding to \mathbf{x} into a medium, sampling template is formed (see Fig. 2.1). The center of such a sampling template is randomly thrown into a medium and corresponding successful hits are computed. Furthermore, if the medium under consideration is statistically isotropic, values found for points located on the same

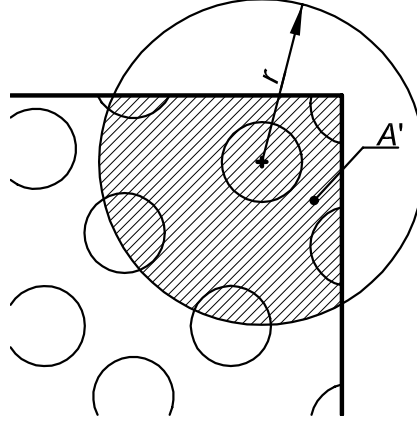


Figure 2.2: Correction factor

circumference can be averaged as well, which allows large number of tests to be performed within one placement of the template.

2.3.2 Functions ρ_n

As stated in Section 2.2.2, the definition of ρ_n -type functions as the probability density functions makes their determination quite complicated. On the other hand, a function which is given as an integral value of function ρ_n can be easily determined. An example of such a function is the second-order intensity function given by Eq. (2.32). According to its definition, function $K(r)$ can be computed as [Axelsen, 1995, Pyrz, 1994]

$$K(r) = \frac{A}{N^2} \sum_{k=1}^N \frac{I_k(r)}{w_k}, \quad (2.45)$$

where $I_k(r)$ is the number of points within a circle with center at particle k and radius r , N is the total number of particles (fibers) in the sample, A is the sample area and w_k stands for correction factor, which takes into account points outside the sampling area if they are not used for the calculation of $I_k(r)$. The correction factor w_k is equal to 1 if periodicity of the microstructure is assumed, otherwise it can be determined as (see Fig. 2.2)

$$w_k = \frac{\pi r^2}{A'}. \quad (2.46)$$

As is evident from Eq. (2.45), for a given microstructure and fixed r , to obtain the value of function K one needs to determine number of points within a distance r from all particle centers in the sample. Provided that particle centers are sorted with respect to one coordinate, this task can be performed by very simple projection method with computational complexity $O(N[\log_2(N) + k])$, where $k \leq N$ (see eg. [Hudec, 1999, Chapter 4]). Therefore, this procedure can perform rather poorly for a very large number of particles, but for the samples under consideration it was found to be sufficiently rapid. Once function $K(r)$ is known, radial distribution function can be determined according to Eq. (2.32) by numerical differentiation of the K function.

The principal disadvantage of functions $K(r)$ and $g_2(r)$ is the fact, that they can be determined by this procedure only for statistically isotropic and ergodic media. Therefore, validity of these hypotheses must be confirmed first before using these functions for the description of a random media.

2.3.3 Microstructural statistics for some theoretical models of microstructures

Now we test proposed methods for two simple cases of statistically isotropic models of microstructure - hexagonal arrangement of particles and model of equisized fully penetrable cylinders. For both configuration, functions $K(r)$ are known in the closed form while the expression for the function $S_{mm}(r)$ was found only for the model of fully penetrable cylinders. In both cases, microstructures are assumed to be periodic.

Hexagonal array of cylinders. The hexagonal arrangement of particles in the matrix can be uniquely specified by the periodic unit cell displayed in the Fig. 2.3. The dimensionless constant ξ is given by

$$\xi^4 = \frac{4\pi^2}{3c_f^2}. \quad (2.47)$$

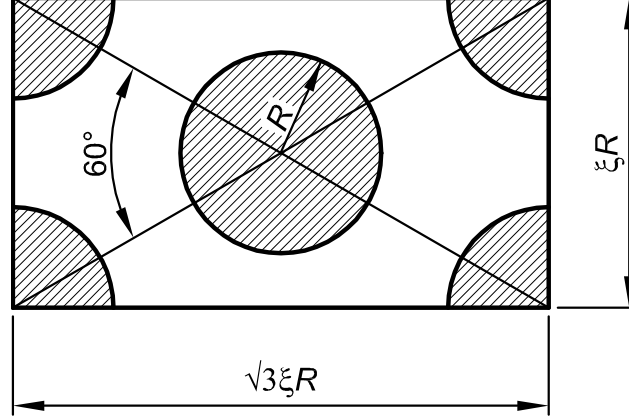


Figure 2.3: Unit cell for hexagonal lattice of fibers

By a simple geometric consideration, function $K(r)$ will have jumps corresponding to regular distances between particles denoted as 1r (corner fibers) and 2r (central fibers),

$${}^1r^2 = \xi^2 R^2 (3i^2 + j^2), \quad (2.48)$$

$${}^2r^2 = \frac{\xi^2}{4} R^2 [3(2i+1)^2 + (2j+1)^2], \quad (2.49)$$

where $i, j = 0, \dots, \infty$. Because there are exactly six additional fibers found for every fiber at a given jump of the function, from Eq. (2.45) we obtain the value of ΔK for every jump in the form

$$\Delta K = \frac{6\pi}{c_f} R^2. \quad (2.50)$$

With the aid of these relations, the value of the function $K(r)$ can be determined for every r . However, to obtain correct results one must carefully inspect the values of 1r and 2r in order to avoid taking one step into consideration twice. The graph of function K for different values of c_f is displayed in Fig. 2.4. Solid lines correspond to values predicted by aforementioned procedure, while dots denote discrete values obtained by numerical procedure.

Fully penetrable cylinders This model assumes that positions of particle centers are totally independent. Thus, value of $\rho_2(r)$ is constant and equal to ρ^2 . Then, $g_2(r) = 1$ and,

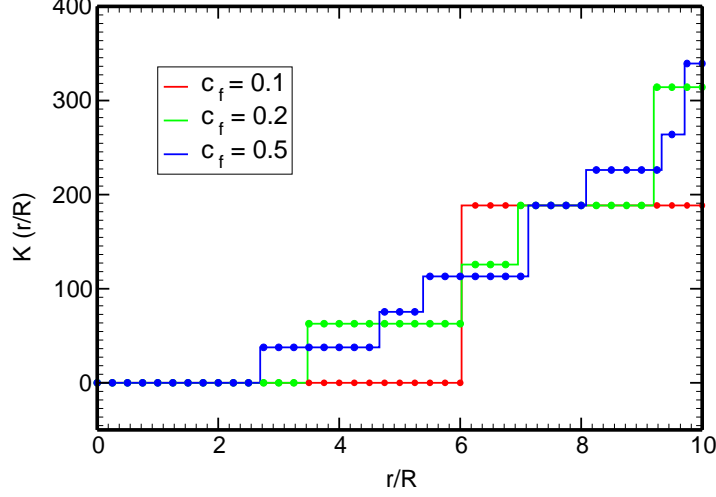


Figure 2.4: Function $K(r)$ for hexagonal packing of fibers

from Eq. (2.32), $K(r)$ is trivially equal to πr^2 .

To determine the value of $S_{mm}(\mathbf{x}, \mathbf{x}')$ one needs to find the probability that union of two cylinders with radius R and centers located in points \mathbf{x} and \mathbf{x}' is not occupied by any particle center. Once we recognize, that this type of microstructure can be described by Poisson probability distribution (see eg. [Rektorys, 1995a, p. 662]) with the intensity $\rho \Omega_u(\mathbf{x}, \mathbf{x}')$, we arrive at the relation

$$S_{mm}(\mathbf{x}, \mathbf{x}') = \exp(-\rho \Omega_u(\mathbf{x}, \mathbf{x}')). \quad (2.51)$$

For the statistically isotropic medium, this expression reduces to [Torquato, 1991]

$$S_{mm}(r) = \exp(-\rho \Omega_u(r)), \quad (2.52)$$

where $\Omega_u(r)$ is the union area of two identical cylinders with radius R and centers separated by distance r . Finally, recognizing that the matrix volume fraction is according to Eq. (2.17) given by

$$S_{mm}(r = 0) = c_m = \exp(-\rho \pi R^2) \quad (2.53)$$

we may determine the number of particles per unit area for the prescribed value of c_m .

To test individual methods we generated 20 different configurations containing 100 particles for fixed value of c_m . For each of these configurations the value of function S_{mm} was determined by template made of concentric circles as displayed in Fig. 2.1 with the number of random throws set to 5,000. $K(r)$ was determined by aforementioned procedure. Results in Fig. 2.5 display averaged value of functions found for particular configurations.

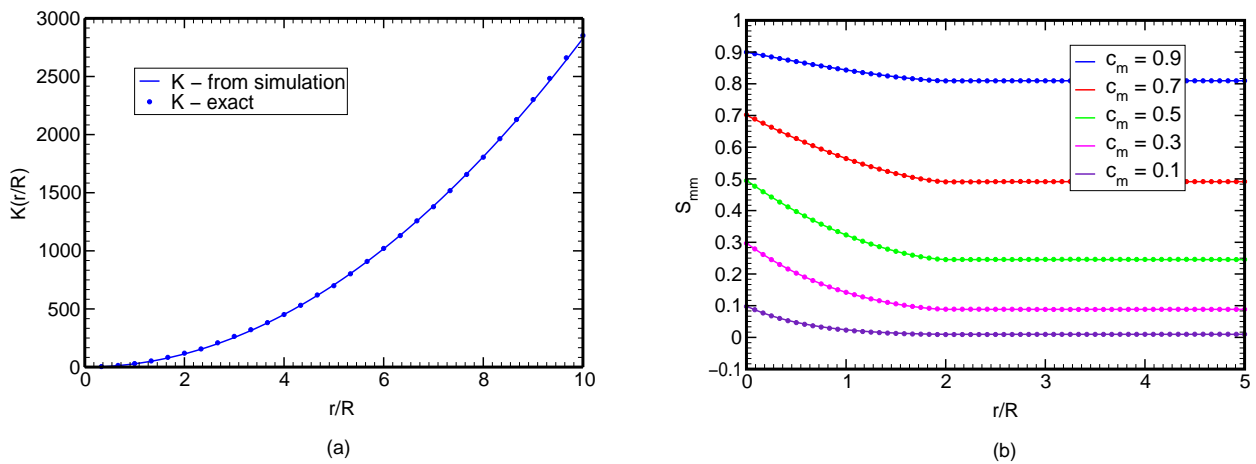


Figure 2.5: Microstructural functions for fully penetrable cylinders.

To conclude, results displayed in Fig. 2.4 and Fig. 2.5 show that proposed methods are sufficiently exact to provide reliable values of given statistical functions.

2.4 Analysis of real microstructure

In this Section, the preceding procedures are applied to the analysis of the micrograph shown in Fig. 1.1. As the first step, the idealized binary image of the micrograph is found using LUCIDA software to determine the radius and position of all particles in the sample. In the following analysis, assumption of statistical homogeneity is applied so every considered micrograph is assumed to be surrounded by periodic replicas of itself.

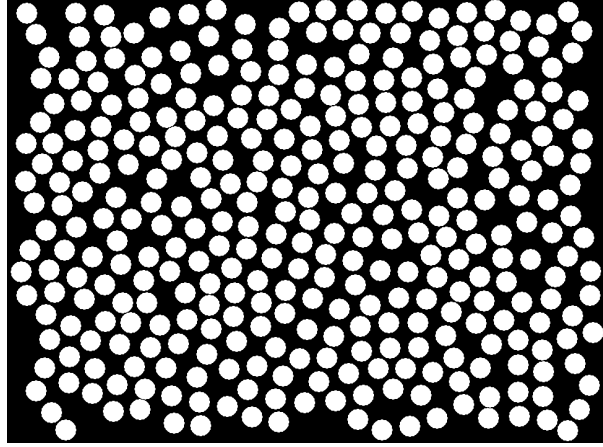


Figure 2.6: Idealized binary image of a transverse cross-section of a fiber tow

Before analyzing the present micrograph, check of the validity of ergodic assumption and the statistical isotropy hypothesis is performed. Provided that these tests justify the assumptions, all previously defined statistical functions can be used for description of the present media.

2.4.1 Testing ergodic hypothesis

To test the ergodic hypothesis it is necessary to form the ensemble space \mathcal{U} . When sampling individual members of \mathcal{U} we started with three micrographs of the fiber tow taken from three specimens at approximately the same location. Each member of the ensemble was then found through a random cut of a part of a given micrograph subjected to condition of the “same” fiber volume fraction. This condition actually supplements the lack of infinity of our composite medium. Fig. 2.7 shows six such individuals generated from the micrograph displayed in Fig. 2.6. In view of the above comments we shall only require that

$$c_r = \frac{1}{n} \sum_{i=1}^n S_r^i, \quad r = f, m, \quad (2.54)$$

where n is the number of members in the ensemble. Functions S_r^i can be derived by randomly placing a point in the member i in a certain number of times while counting the number

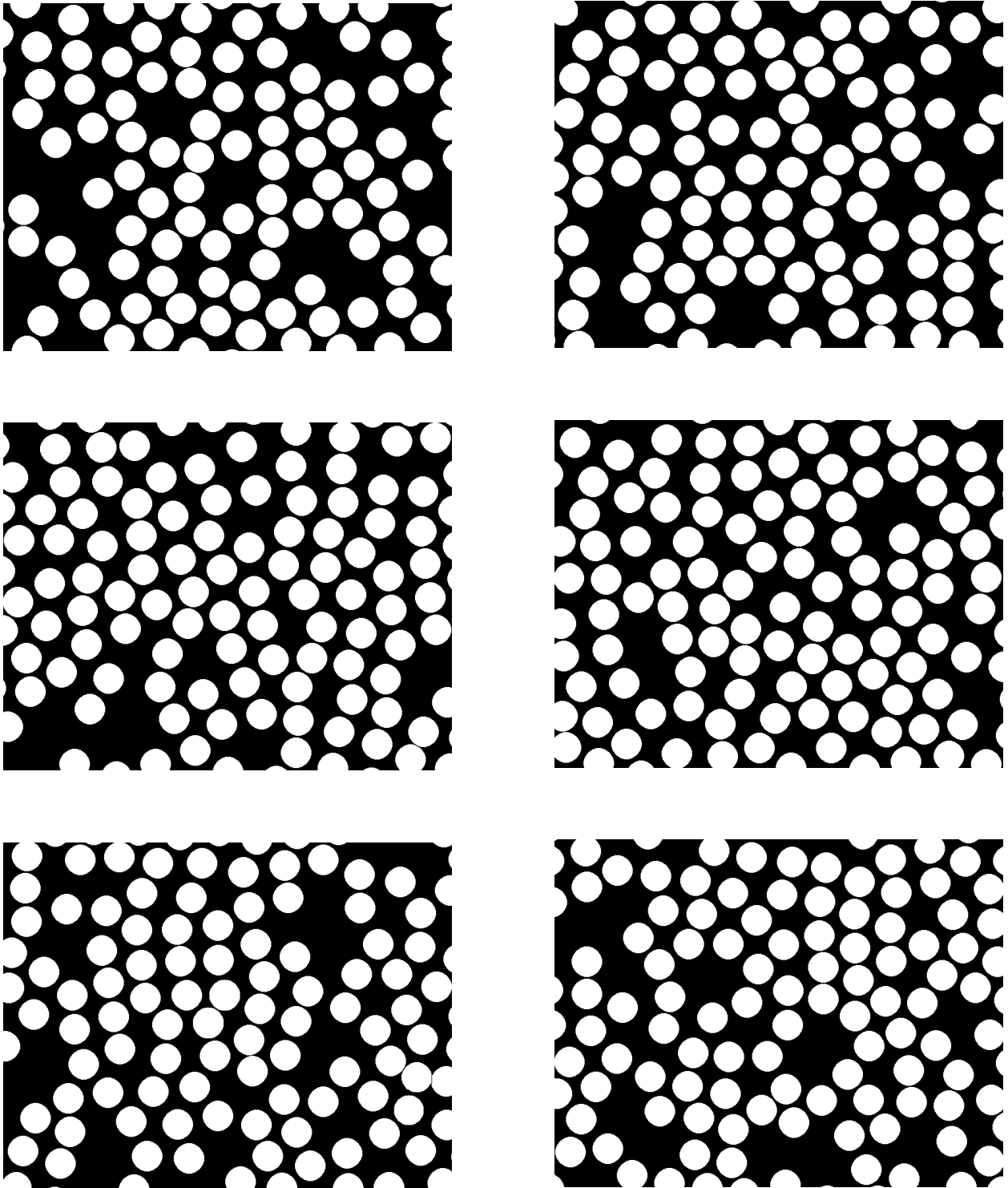


Figure 2.7: Selected members of the sample space

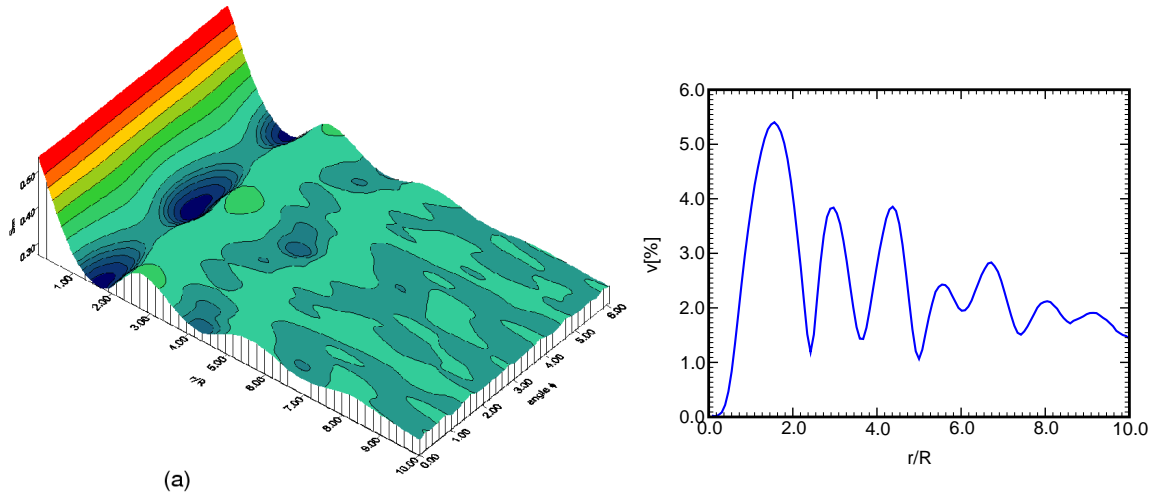


Figure 2.8: Two-point matrix probability function $S_{mm}(\mathbf{x} - \mathbf{x}')$ and variation coefficient $v(\phi)$ of $S_{mm}(r, \phi)$ plotted as a function of r/R .

of hits in the phase r and then dividing by the total number of throws. When setting the number of throws equal to 500 we found $\overline{S_f} = 0.42$, which agrees well with the average fiber volume fraction $\overline{c_f} = 0.435$. A better agreement can be expected for larger n . Although an ultimate justification of an ergodic assumption would require to prove equality of higher moments as well, we argue that the presented results are sufficient for the medium to be considered as ergodic, providing the medium is indeed statistically homogeneous. In the sense of an ergodic assumption we suggest that a single micrograph can be used hereafter for evaluation of the required statistical descriptors.

2.4.2 Test of statistical isotropy

To check the statistical isotropy of the medium under consideration we plotted the distribution of the two-point matrix probability function S_{mm} for a statistically uniform medium as a function of the absolute difference of points \mathbf{x} and \mathbf{x}' and orientation ϕ , Fig. 2.8(a). These results were obtained by 100,000 random throws of sampling template shown in Fig. 2.1. Should the material be statistically isotropic (independent of orientation) the variation coef-

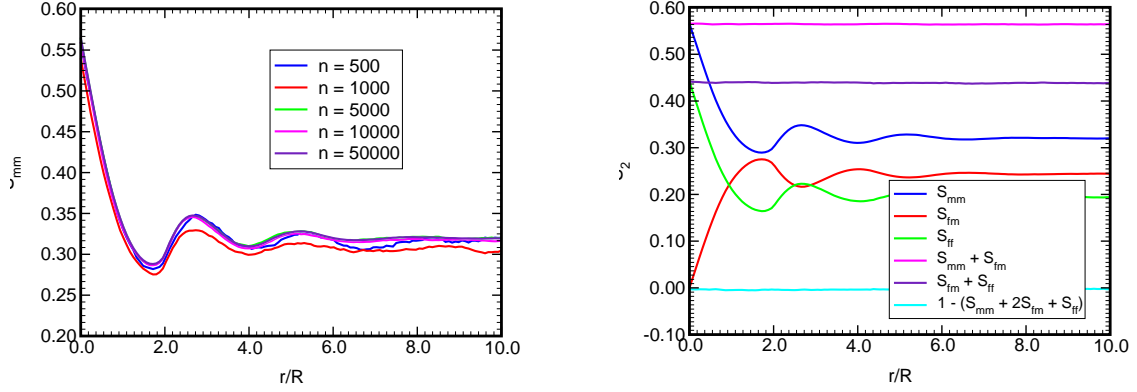


Figure 2.9: Two-point matrix probability $S_{mm}(r)$ and unique relations for the general two-point probability function $S_{rs}(r)$.

ficient $v(\phi)$ of $S_{mm}(\phi)|_{r/R}$ for a given ratio r/R would be equal to zero. For the purpose of our next study, however, the material shall be treated as statistically isotropic, and the maximum 5% variation evident from Fig. 2.8(b) is taken as an acceptable error of the assumption.

2.4.3 Microstructure describing functions

Once all the assumptions were verified to some extent, all microstructure describing functions can be determined for the current microstructure.

Two-point probability functions. First, the effect of the number of random throws on the value of function S_{mm} was inspected. Results appear in Fig. 2.9(a). It is evident that for the present microstructure 5,000 repetitions are sufficient, which represent approximately 1 minute long computation for PC computer with Intel Pentium 200MMX processor. Fig 2.9(b) further shows certain unique relationships for the isotropic and ergodic medium, which are based on relations given in Table 2.1. As evident, proposed relations hold very well. Therefore obtained functions are sufficiently precise.

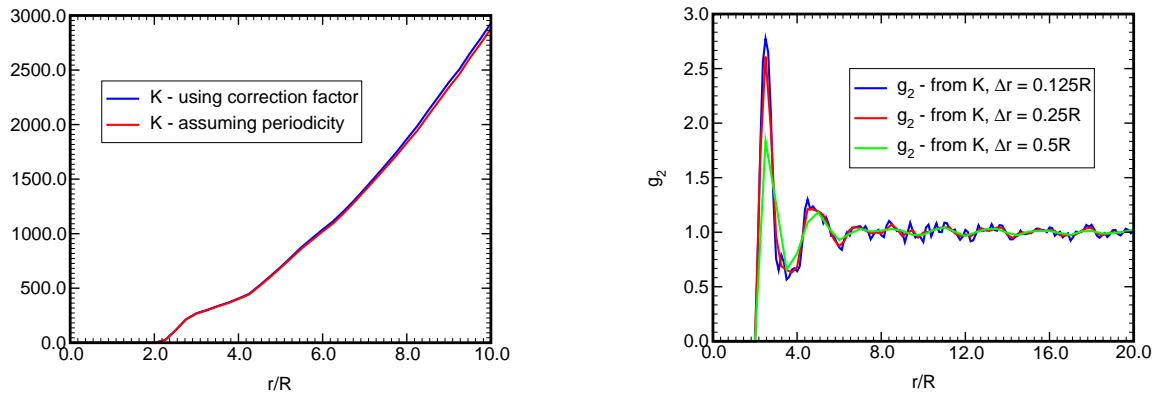


Figure 2.10: Second order intensity function $K(r)$ and radial distribution function $g_2(r)$

The two-particle probability density based functions. We start with the determination of function $K(r)$. Results are shown in Fig. 2.10(a) for the determination of $K(r)$ with the help of correction factor and periodicity conditions. The slight declination of curves shows that results obtained by correction factor are partially biased, especially for larger values of r . Even bigger differences are expected to be found for micrographs with a smaller number of particles.

The function $g_2(r)$ was determined from function $K(r)$ by numerical differentiation. Results displayed in Fig. 2.10(b) are found by central difference formula with various values of steps used for numerical differentiation. As it can be anticipated, obtained results are strongly dependent on the step size, furthermore for smaller values of Δr function oscillates substantially.

Finally, the relation between function S_{mm} and functions $K(r)$ and $g_2(r)$ is inspected. To evaluate integrals (2.42, 2.43), adaptive Simpson's integration scheme was used (see [Burden and Faires, 1989]) with prescribed tolerance 10^{-4} . Results shown in Fig. 2.11 are obtained from $K(r)$ or $g_2(r)$ functions and simulation for 50,000 repetitions of sampling

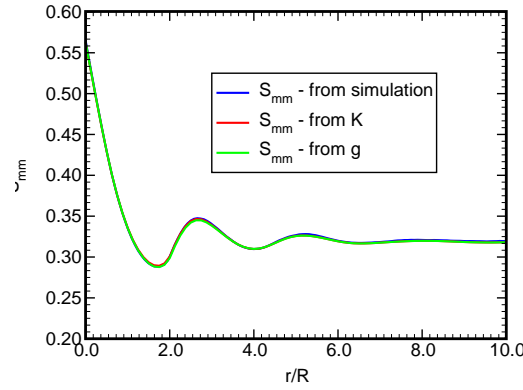


Figure 2.11: The two-point matrix probability function

procedure. Coincidence of individual curves is evident. It is necessary to note that this procedure took approximately only 1 second on PC computer with Intel Pentium 200MMX processor, when most of the time computation was consumed by the numerical integration. The time needed for the determination of function $K(r)$ itself was negligible.

2.4.4 Conclusions

To conclude, the medium under the consideration was tested to some extent for the ergodic assumption and for the statistical isotropy. These hypotheses were confirmed for the current micrograph of a unidirectional fiber tow. The relation between presented functions makes possible to choose any of these functions as a basic statistical descriptor; in the foregoing optimization procedure the *function $K(r)$ will be considered as the basic microstructure describing function*, because its evaluation is the quickest from all the functions mentioned heretofore.

Chapter 3

CONSTRUCTION OF THE PERIODIC UNIT CELL

In Chapter 2, microstructure characterizing functions were identified and their applicability to the current microstructure description was examined. This Chapter is devoted to the principle objective of this work - determination of the periodic unit cell, which possesses similar statistical properties as the original microstructure. Similarity of these two materials in terms of microstructure configuration is measured by some objective function incorporating a certain statistical descriptor.

Section 3.1 defines such a objective function using the second order intensity function $K(r)$ as a basic statistical descriptor of the media and certain geometrical parameters of the unit cell (location of the particle centers and dimensions of the unit cell) as a free parameters of this function. The process of finding the minimum value of the objective function is divided into two steps - finding the optimal positions of fibers for fixed dimension of the unit cell and then finding the optimal dimensions of the unit cell. The second step of this procedure represents the one-dimensional minimization problem, which can be easily solved by an elementary optimization procedure. However, to solve the first step, minimization of multi-dimensional, multi-modal function with a large number of local minima must be performed, which is a very difficult task itself. A variety of deterministic and stochastic algorithms is tested in Sections 3.2 and 3.3., respectively. Section 3.4 presents some additional improvements relating to stochastic optimization procedures. Finally, Section 3.5 is devoted to the determination of resultant unit cells.

3.1 Objective function and problem definition

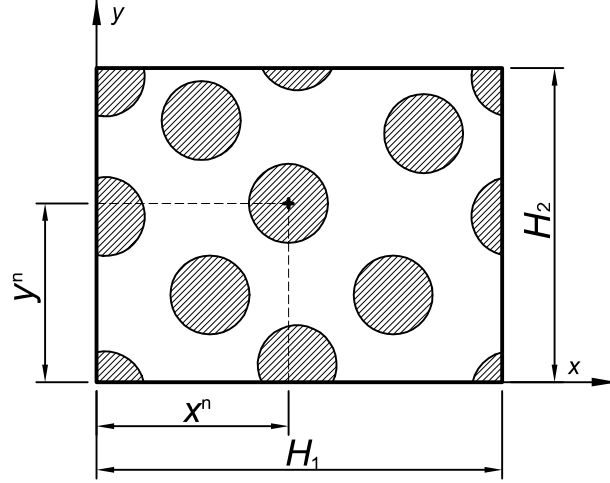


Figure 3.1: Geometry of the periodic unit cell

Consider the periodic unit cell consisting of N particles displayed in Fig. 3.1. The geometry of such a unit cell is determined by the values of dimensions H_1 and H_2 of the unit cell and x and y coordinates of all particles. The principal problem now is to select these values in such a way that material formed by this periodic unit cell is as much similar to some given original microstructure as possible. In order to be able to quantify the similarity between two distinct microstructures, it is convenient to introduce certain objective function which incorporates some characteristics pertinent to both microstructural configurations.

The relevant characteristics can be in the present context provided by any microstructure describing functions, presented in Chapter 2. For the current situation, the objective function is chosen to be

$$F(\mathbf{x}^N, H_1, H_2) = \sum_{i=1}^{N_m} \left(\frac{K_0(r_i) - K(r_i)}{\pi r_i^2} \right)^2, \quad (3.1)$$

where vector $\mathbf{x}^N = \{x^1, y^1, \dots, x^N, y^N\}$ stands for the position of particle centers of the periodic unit cell, x^i and y^i correspond to x and y coordinates of the i -th particle, H_1 and H_2 are the dimensions of the unit cell, $K_0(r_i)$ is the value of K function corresponding to

the original media calculated in point r_i and N_m is the number of points, in which both functions are evaluated.

The choice of function $K(r)$ for the optimization problem is primarily attributed to its simplicity and a very rapid evaluation for a reasonable number of particles N . In addition, the selected form of the objective function F (namely the “normalization” term πr^2), Eq. (3.1), is quite useful since it serves directly as a “natural” penalization when particles happen to overlap. Therefore, no additional algorithmic labor necessary for avoiding unacceptable solutions [Povirk, 1995] is needed if the material is formed by impenetrable particles.

To find the optimal periodic unit cell the values of \mathbf{x}^N , H_1 and H_2 which provide the minimum value of function F must be determined. To solve this problem in its fully generality is prohibitively difficult; therefore it is convenient to split the minimization procedure in two separate problems, namely:

Optimal fiber configuration. For a given number of fibers N , dimensions of a unit cell H_1 and H_2 and values of the original function $K_0(r)$ evaluated in points r_i , $i = 1, \dots, N_m$ find the configuration of particle centers $\mathbf{x}^N(H_1, H_2)$ such that:

$$\mathbf{x}^N(H_1, H_2) = \arg \min_{\mathbf{x}^N \in \mathcal{S}} F(\mathbf{x}^N, H_1, H_2), \quad (\text{P1})$$

where \mathcal{S} denotes a set of admissible vectors \mathbf{x}^N .

The noteworthy feature of this formulation is that the set \mathcal{S} of admissible vectors can be defined in different ways as is advantageous for a given optimization procedure:

- When we take into account the periodicity of the unit cell the individual components of vector \mathbf{x}^N can take arbitrary values so the problem can be treated as an *unconstrained* one.
- Another possibility is to restrict the position of fibers only to unit cell by

$$0 \leq x^i \leq H_1, \quad 0 \leq y^i \leq H_2, \quad i = 1, \dots, N, \quad (3.2)$$

so the problem becomes *bound-constrained*.

- Finally, in Section 3.4.2 the *impenetrability condition* will be imposed, which with the use of some additional tricks results in substantial improvement of the optimization procedure performance.

Once this problem is solved, the only unknown parameters are the values of H_1 and H_2 . Furthermore, if we require that the periodic unit cell must have the same volume fraction of phases c_r as the original microstructure, the problem reduces to finding the optimal ratio $\eta = H_1/H_2$ only. Thus, the second problem can be stated as

Optimal ratio H_1/H_2 . For known values of $\mathbf{x}^N(\eta)$ and for fixed volume fraction of phases, find the value of ratio η^N such that:

$$\eta^N = \arg \min_{\eta \in \langle \eta_a; \eta_b \rangle} F(\mathbf{x}^N(\eta)), \quad (\text{P2})$$

where values η_a and η_b should be chosen to cover all the reasonable dimensions of the unit cell.

While problem (P2) presents one-variable function optimization problem only, solving the problem (P1) requires to locate the global minimum of multi-dimensional function. Moreover, for the present problem the function F is a multi-modal, noisy, with a large number of plateaus and local minima (see Fig. 3.2(b)). This further complicates the situation. Therefore, we first turn our attention to the solution of problem (P2); various approaches developed for solving the problem (P1) are discussed in Sections 3.2–3.4.

Let us suppose for the moment, that we are able to solve the problem (P1). Then, the simplest algorithm suitable for one-dimensional optimization is the *Golden Section search* method [Press et al., 1992, Chapter 10.1]. Roughly speaking, given initial triplet of points a, b, c this algorithm is based on generating a new point in locations, which divide intervals $\langle a; b \rangle$ or $\langle b; c \rangle$ in some prescribed ratio – Golden section. The new point then replaces one of the points a, b, c according to its function value and position. The principle of this method is shown in Algorithm 3.1.

```

1  supply values  $a < b < c$  such that  $f(a) > f(b) \wedge f(c) > f(b)$ 
2  while(( $c - a$ ) <  $\epsilon$ ) {
3      determine new point  $d$ 
4      if ( $f(d) < f(b)$ )
5           $b = d$ , update  $a, c$  with respect to step 1
6      else
7          if( $d < b$ )  $a = d$ 
8          else  $c = d$ 
9  }
```

Algorithm 3.1: Golden Section search

Step 1 The initial points a and b corresponds in the present context to values η_a and η_b in (P2) and the function value $f(\cdot)$ represents here the minimum value of function F found for the optimization problem (P1) for given side ratio.

Step 3 The new point is located in the larger of two intervals $\langle a; b \rangle$ and $\langle b; c \rangle$, its distance from point b is $(3 - \sqrt{5})/2$ times the length of larger interval.

For all computations performed here, the parameters η_a and η_b were set to 1.0 and 2.0 respectively.

To check, whether the values η_a and η_b are consistent with the requirements of the step 1 of Algorithm 3.1, let us recall the results obtained in Section 2.3.3 for function $K(r)$ associated with the hexagonal packing of fibers. As was shown here, every regularity of microstructure results in the jump of function $K(r)$ with the amplitude corresponding to the number of fibers located at the same distance from a given particle. Therefore, for the side ratio $\eta = 1.0$ as well as for $\eta = 2.0$ and eg. for values of $r = iH_1$, $i = 1, \dots, \infty$, four

other fibers are always found, while this situation does not occur for the intermediate values of η . Because function $K(r)$ relevant to the original microstructure does not possess such jumps (see Fig. 2.10) the value of function F for $\eta \in (1; 2)$ should be always smaller than for the interval endpoints.

3.2 Deterministic algorithms

In previous Section, the procedure for the determination of periodic unit cell was established provided that we are able to find the optimal fiber configuration for given size of a unit cell. Some commonly used deterministic optimization procedures will be presented here to obtain the solution of problem (P1).

The most widely used approach for finding the global minimum relies on restarting the optimization procedure from widely varying points [Press et al., 1992, p. 394] and then identify the lowest value of function found as a global minimum. In [Yuret, 1994] simple method was proposed to enhance this procedure. Instead of the random determination of starting points it rather explores the portions of search space far from previously found local minima in order to avoid trapping into the same minimum again. The method is summarized in Algorithm 3.2, where \mathcal{X} corresponds to a set of obtained solutions, \mathbf{L} and \mathbf{U} correspond to vector of lower and upper bounds for given components of \mathbf{x} .

The *LocalOptimize* procedure in Step 4 of Algorithm 3.2 corresponds to a given optimization algorithm. In the present work, three methods were tested - namely Dynamic Hill Climbing, Powell's method and BFGS algorithm were implemented. Because all these local optimizers are formulated for the case of *unconstrained optimization* problem, periodicity of the unit cell is taken into account to allow individual components of vector \mathbf{x}^N to take arbitrary values.

Finally, self-explanating Algorithm 3.3 shows procedure for generating the distant points used in this work.

```

1   $\mathcal{X} = \{\mathbf{L}, \mathbf{U}\}$ 
2  while (not termination-condition) {
3       $\mathbf{x}_0 = \text{Distant\_point}(\mathcal{X})$ 
4       $\mathbf{x} = \text{Local\_optimize}(\mathbf{x}_0)$ 
5       $\mathcal{X} = \mathcal{X} \cup \mathbf{x}$ 
6  }
```

Algorithm 3.2: Principle of deterministic optimizations

```

1  for each dimension  $d$  {
2      sort  $\mathbf{x}_i \in \mathcal{X}$  by  $\mathbf{x}_i[d]$ 
3      find  $j : (\mathbf{x}_j[d] - \mathbf{x}_{j-1}[d])$  is maximal
4       $\mathbf{x}[d] = u(\mathbf{x}_{j-1}[d], \mathbf{x}_j[d])$ 
5  }
```

Algorithm 3.3: The *Distant_point* algorithm

3.2.1 Powell's method (POWELL)

The principle of Powell's method is to perform sequence of one-dimensional line-minimization (similar to the one given by Algorithm 3.1) along the set of given directions, typically taken as unit vectors. However, in the numerical tests performed here the modification of this classical approach based on heuristic choice of minimization direction (see [Press et al., 1992, Chapter 10.5] for details) was used.

3.2.2 Dynamic Hill Climbing (DHC)

Another non-derivative based method is the Dynamic Hill Climbing procedure proposed by Yuret. This method combines certain heuristic rules to enhance the performance of optimization - variable length of a step size, which expands when better solutions are found and shrinks when no progress is made, combined with short-term memory. For the more information inspect [Yuret, 1994].

3.2.3 BFGS method

Finally, the **BFGS** method was chosen as a representative of a gradient-based methods. The implementation of this method was again taken from [Press et al., 1992, Chapter 10.7]. The values of gradients were obtained here by forward difference formula with step $\Delta h = \varepsilon x^i$ or $\Delta h = \varepsilon y^i$ respectively.

3.2.4 Test example

To test individual methods we assumed a square periodic unit cell consisting of 10 fibers with the same volume fraction as the real specimen. The function $K_0(r)$ and $K(r)$ were fitted in five points ($N_m = 5$). Sampled points were spaced by fiber diameter. Each algorithm with parameters displayed in Appendix B, Table B.1 was run 20 times. The iteration process was terminated, if one of the following conditions was met:

- Algorithm returned value $F(\mathbf{x}) \leq \varepsilon = 6 \times 10^{-5}$.

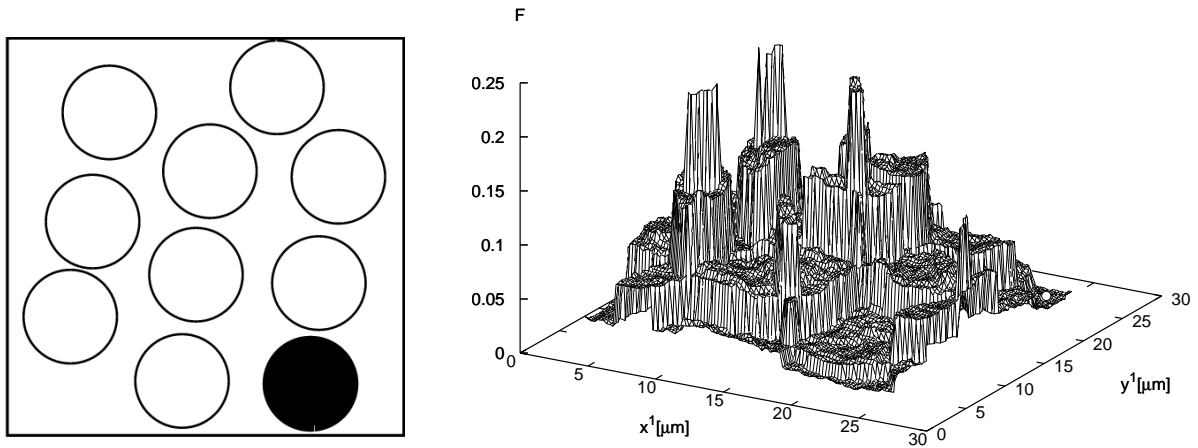


Figure 3.2: An admissible unit cell

- Number of function evaluations exceeded 250,000.
- Number of discovered local minima exceeded 10,000.

For each run the number of function evaluations was recorded together with the minimum attained value of the objective function.

To manifest the problem complexity, an admissible unit cell consisting of 10 fibers together with an example of the objective function F is shown in Fig. 3.2. Coordinates x^1 and y^1 on Fig. 3.2(b) represent locations of the filled fiber center. Positions of remaining fibers are fixed. The minimum of function F for the present configuration is marked by a hollow circle.

Results and discussion. Table 3.1 shows the minimum, maximum, and average of minima found by different local optimization procedures. These values show that the performance of all methods for the current problem is quite poor. The worst result is delivered by the **BFGS** method, which was unable to locate the prescribed value of the objective function for all runs. This fact is probably caused by the presence of plateaus found in our objective function (see Fig. 3.2(b)) where derivatives of the objective function vanish. The

performance of Powell's method is slightly better since the returned values of the objective function are substantially smaller than for **BFGS** algorithm. However, this method still succeeded only once in finding the required value of the objective function. The **DHC** method is clearly the most succesfull of all proposed methods. Still, the chance like 1:3 of locating the presribed value of the objective function is simply not satisfactory. Moreover, to obtain such results, quite large number of function evaluations must be performed (see Table 3.2). To reduce this quantitiy it is necessary to provide more promising starting points \mathbf{x}_0 than those supplied by Algorithm 3.3.

3.3 Stochastic optimization methods

Results obtained in the previous Section imply that to locate the global minimum of the current objective function, it is necessary to explore the search space \mathcal{S} more thoroughly instead of starting a determininstic optimizer from a quasi-randomly generated points.

A variety of stochasic methods uses such an approach. In the sequel, a number of the *evolutionary algorithms* is formulated to solve given optimization problem. Namely four different modifications of a *simple genetic algorithm* and method of *differential evolution* is adressed. Moreover, the algorithm based on a *simulated annealing* procedure is proposed here. At the end, the performance of these algorithms is compared with those presented in the previous Section.

To define search space \mathcal{S} one may now adopt the second option mentioned in Section 3.1

Algorithm	Number	Returned value $\times 10^5$		
	found	Min	Avg	Max
POWELL	1/20	6.0	34.9	122.3
DHC	7/20	5.9	9.7	25.4
BFGS	0/20	2030.8	6992.5	11617.3

Table 3.1: Minimum values of function

Algorithm	Number of evaluations		
	Min	Avg	Max
POWELL	244,258	244,258	244,258
DHC	99,128	147,706	216,586
BFGS	-	-	-

Table 3.2: Number of function evaluations for deterministic optimizers

and restrict the position of fibers to the area of the unit cell only.

3.3.1 Principle of genetic algorithm

Genetic algorithms (GAs), as stated in the introductory part, are formulated using a direct analogy with evolution processes observed in nature, a source of fundamental difference between traditional optimizers and GAs.

Genetic algorithms, in contrast to traditional methods presented in the previous Section, work simultaneously with a population of individuals, exploring a number of new areas in the search space in parallel, thus reducing a probability of being trapped in a local minimum. As in nature, individuals in a population compete with each other for surviving so that fitter individuals tend to progress into new generations, while the poor ones usually die out. This process is briefly described in Algorithm 3.4.

Algorithm 3.4 provides basic steps of a single GA cycle; reproduction phase (step 5), recombination (step 6), and selection of a new population (step 7). In the next Subsection we first explore mechanisms of selections of new individuals, which undergo genetic process (step 5), and then we proceed with basic operators controlling the step 6. Steps 5 and 7 will be explained in more details when formulating various algorithms for solving the optimization problem.

```

1   $t = 0$ 
2  generate  $P_0$ , evaluate  $P_0$ 
3  while (not termination-condition) {
4       $t = t + 1$ 
5      select  $M_t$  from  $P_{t-1}$                 (apply sampling mechanism)
6      alter  $M_t$                             (apply genetic operators)
7      create  $P_t$  from  $M_t$  and evaluate  $P_t$     (insert new individuals into  $P_t$ )
8  }
```

Algorithm 3.4: Principle of genetic algorithm

3.3.2 Sampling mechanisms

In step 5 of Algorithm 3.4 individuals selected for the reproduction are copied to the “mating” pool according to their relative performance referred to as their “fitness”, or “figure of merit”. In the case of function optimization it is simply equal to the function value or rather its inverse when solving minimization problem. An expected number of copies each individual should receive in the mating pool M_t is given by

$$e_i = \frac{s_i}{\sum_{j=1}^P s_j} M, \quad s_i = \frac{1}{\delta + f_i}, \quad f_i \geq 0 \quad (3.3)$$

where P is the number of individuals in the population M is the number of individuals in a mating pool M_t and f_i is the function value associated with the i -th individual; $s_i = f_i$ when solving maximization problem. Parameter δ is a small positive number which prevents division by zero. The procedure which allocates the new individuals into mating pool M_t according to Eq. (3.3) and thus turns expected number of offspring (which is a real number) into provided number of offsprings (which is a integer number) is called *sampling mechanism*. In the sequel the procedures used to perform this step are summarized.

Fitness scaling. Usually it is not desirable to sample individuals according to their raw fitness. In such a case the best individuals may receive a large number of copies in a single generation, so after a small number of GA cycles all individuals start to look alike and the algorithm usually converges prematurely to a local minimum. To compress the range of fitness a *linear scaling* (shifting) of the fitness function is incorporated into sampling procedures [Goldberg, 1989]. Then, the relation between the raw fitness s and the scaled fitness s' is simply $s' = as + b$. The standard procedure for the determination of constants a and b is to require the average raw fitness s_{avg} and scaled fitness s'_{avg} to be the same. The second condition is then provided by prescribing the value of maximal scaled fitness by $s'_{\text{max}} = C_{\text{mult}} s'_{\text{avg}}$, where the values $C_{\text{mult}} \in \langle 1.2; 2 \rangle$ are usually used.

Roulette wheel selection. In this method the probability of selecting i -th individual is set to $p_i = s'_i / \sum_{j=1}^P s'_j$. As the first step of a selection, a real number p with uniform distribution on the interval $\langle 0; 1 \rangle$ is generated and then the first individual for which its *cumulative probability* $\sum_{i=1}^j p_i$ exceeds p is inserted into the mating pool. This procedure is repeated until the mating pool is full. More details can be found in [Goldberg, 1989, Kvasnička, 1993].

Note that this procedure is often described as an analogy of a single spin of roulette wheel with one marker, where parts of wheel corresponding to individual members are allocated with respect to the value p_i .

Stochastic universal sampling (SUS). Stochastic universal sampling is a generalization of previous selection method proposed by Baker in [Baker, 1987]. The standard roulette wheel is marked with equally spaced pointers indicating the happy individual selected for reproduction. A number of pointers indicates a number of desired individuals used for reproduction, which are again obtained by the single spin of roulette wheel.

Remainder Stochastic Independent Sampling (RSIS). [Baker, 1987] This method firstly allocates individuals according to the integer part of their e_i . Then, to sample the

fractional parts, we first generate a random real number r uniformly distributed within the range $\langle 0; 1 \rangle$. Then we check, whether the fractional part of the i -th individual is greater than r . If yes, the individual is added to the mating pool and its fractional part is set equal to zero. If not, we move to the next individual. These steps are repeated until the number of individual in the mating pool equals M .

For the sake of completeness we also briefly mention two selection methods which are not based on the expected number of copies in mating pool each individuals should receive. The main advantage of this approach is that it principally prevents the best individuals from causing the premature convergence of the whole population.

Tournament selection. Whenever an individual is to be selected to the mating pool, two individuals are picked randomly from the original generation. Then the individual with higher fitness is copied into the mating pool. This procedure is repeated until the mating pool is full. More details about this procedure can be found in [Beasley et al., 1993a].

Normalized geometric ranking. In this method, the probability of individual's selection is based on its *rank* or *position* in the population rather than on the value of fitness. For this particular method (see [Houck et al., 1995]), probabilities are assigned to each individual exponentially and are normalized to provide the cumulative probability of selection equal to 1. Thus, the probability of selection of i -th individual is

$$p_i = q'(1 - q)^{r-1},$$

where q is the probability of selecting the best individual in the population, r is the rank of i -th individual with respect to its raw fitness, and $q' = q/(1 - (1 - q)^P)$.

3.3.3 Genetic operators

Let us now proceed with step 6 of Algorithm 3.4, where individual members of the population breed in order to combine their (we hope) good characteristics to produce (we hope) a better

offspring.

To accomplish this procedure, solution vector \mathbf{x}^N must be transformed into the genetic information - *chromosome* formed by sequence of *genes*. Then the mating process is provided by applying the *genetic operators* to the individual members of population. In the classical version of genetic algorithm [Goldberg, 1989] the chromosomes are represented by binary numbers and only two basic operators are used - single-point crossover and mutation. Unfortunately, this representation is not suitable for the considered problem where the solution is formed by multi-dimensional real vectors. To encode this vector into binary representation with a reasonable precision, huge chromosome must be used, which leads to the poor performance of the algorithm.

In view of this general conclusion we now abandon the binary representation of parameters and turn our attention to a floating-point representation of genes instead. This step brings a number of advantages. First of all, using real numbers easily allows representation to the machine precision. In addition, the search operators work directly in the search domain thus no mapping between the representation space and the search space is required. This is a direct consequence of the floating point implementation, where each chromosome vector is coded as a vector of floating point numbers, of the same length as the solution vector. Particularly, each individual – a configuration of particles in the unit cell – is represented by a real-valued chromosome $\mathbf{X} = \{x_1, \dots, x_{2N}\}$. Individual components of this vector are related to actual fiber centers as follows

$$x_{2i-1} = x^i \quad \text{and} \quad x_{2i} = y^i \quad \text{for } i = 1, \dots, N,$$

where N is the number of fibers within the unit cell, x^i and y^i represent the x and y coordinate of i -th particle.

Moreover, different representation of genes calls for the suitable choice of genetic operators. Michalewicz in [Michalewicz, 1992, Michalewicz et al., 1994] proposed a group of real-valued genetic operators which are formulated for the convex search space \mathcal{S} , so they can be directly used for the solution of considered problem. The description of these opera-

tors follows.

Let L_i and U_i represent the lower and upper bound for each variable x_i , respectively. Further assume that vector \mathbf{X} represents a parent, whereas vector \mathbf{X}' corresponds to an offspring; $u(a, b)$ is a real number and $u[a, b]$ is an integer number with uniform distribution defined on a closed interval $\langle a; b \rangle$. The following operators can be now defined:

Uniform mutation: Let $j = u[1, 2N]$ and set:

$$x'_i = \begin{cases} u(L_i, U_i), & \text{if } i = j \\ x_i, & \text{otherwise} \end{cases}$$

Boundary mutation: Let $j = u[1, 2N]$, $p = u(0, 1)$ and set:

$$x'_i = \begin{cases} L_i, & \text{if } i = j, p < .5 \\ U_i, & \text{if } i = j, p \geq .5 \\ x_i, & \text{otherwise} \end{cases}$$

Non-uniform mutation: Let $j = u[1, 2N]$, $p = u(0, 1)$ and set:

$$x'_i = \begin{cases} x_i + (L_i - x_i)f(t), & \text{if } i = j, p < .5 \\ x_i + (U_i - x_i)f(t), & \text{if } i = j, p \geq .5 \\ x_i, & \text{otherwise} \end{cases}$$

where $f(t) = u(0, 1)(1 - t/t_{max})^b$, t is the current generation, t_{max} is the maximum number of generations and b is the shape parameter. This operator allows for a local tuning as it searches the space uniformly initially and very locally at later stages.

Multi-non-uniform mutation: Non-uniform mutation applied to all variables of \mathbf{X} .

Simple crossover: Let $j = [1, 2N]$ and set:

$$x'_i = \begin{cases} x_i, & \text{if } i < j \\ y_i, & \text{otherwise} \end{cases}$$

$$y'_i = \begin{cases} y_i, & \text{if } i < j \\ x_i, & \text{otherwise} \end{cases}$$

Simple arithmetic crossover: Let $j = u[1, 2N]$, $p = u(0, 1)$ and set:

$$x'_i = \begin{cases} px_i + (1-p)y_i, & \text{if } i = j \\ x_i, & \text{otherwise} \end{cases}$$

$$y'_i = \begin{cases} py_i + (1-p)x_i, & \text{if } i = j \\ y_i, & \text{otherwise} \end{cases}$$

Whole arithmetic crossover: Simple arithmetic crossover applied to all variables of \mathbf{X} .

Heuristic crossover: Let $p = u(0, 1)$ and set:

$$\mathbf{X}' = (1+p)\mathbf{X} - p\mathbf{Y}$$

$$\mathbf{Y}' = \mathbf{X}$$

where \mathbf{X} is better individual than \mathbf{Y} in terms of fitness. If $\mathbf{X}' \notin \mathcal{S}$, then a new random number p is generated until the feasibility condition ($\mathbf{X}' \in \mathcal{S}$) is met or the maximum allowed number of heuristic crossover applications is exceeded.

Now when the principal steps of genetic algorithms were explored we proceed with four particular examples of genetic algorithm. For each of these algorithms, relevant steps of Algorithm 3.4 are discussed more thoroughly.

3.3.4 Genetic algorithm I (GA I)

Let us start with the most simple one usually termed as *Steady State GAs*. Reproduction is implemented through the weighted roulette wheel and only one or two offspring are created within each generation. For better understanding we now review the relevant steps:

Step 5 By spinning the roulette wheel select the r individuals from population P_{t-1} required for mating (one individual for mutation, two individuals when the crossover operator is applied). These individuals are temporarily stored in the mating pool M_t . Linear scaling is used to reduce a common threat of premature convergence to a local optimum.

Step 6 Altering M_t by applying either crossover or mutation operators. In our case, the mutation operators are used twice as often as the crossover operators.

Step 7 Based on a number of new offspring created select a corresponding number of individuals from P_{t-1} to die using the inverse roulette wheel. Insert new offspring into P_{t-1} to create P_t .

3.3.5 Genetic algorithm II (GA II)

This algorithm closely resembles the simple genetic algorithm described in [Goldberg, 1989] with only minor changes. To reduce statistical errors associated with the roulette wheel selection the *Remainder Stochastic Independent Sampling* procedure is employed in this case. As for **GA I** we now review the important steps of Algorithm 3.4:

Step 5 By applying the **RSIS** sample individuals from P_{t-1} and copy them into the mating pool M_t . Note that precisely P individuals are selected for reproduction. This sampling method thus falls into category of preservative and generational selections according to the classification of [Michalewicz, 1992]. Similar actions as in **GAR I** are taken to deal with the premature convergence.

Step 6 Genetic operators are applied to *all* individuals in M_t . Each operator is used in a prescribed number of times depending on the population size, and new individuals are placed into a temporary population P'_t . Parents for breeding are selected uniformly.

Step 7 Create a new population P_t by successively replacing the worst individual from P_{t-1} by individuals from the temporary population P'_t .

3.3.6 Genetic algorithm III (GA III)

This algorithm is essentially a replica of the Michalewicz modGA algorithm presented in [Michalewicz, 1992, p. 59]. It employs the *stochastic universal sampling mechanism* because it allows us to select arbitrary number of individuals to the mating pool by a single wheel spinning. This is particularly appreciable when applying the modGA, which is characterized by following steps:

Step 5a Using the **SUS** select a subset of n individuals from P_{t-1} for reproduction and copy them to M_t . Note that each member of M_t can appear only once in the reproduction cycle.

Step 5b Again using the **SUS** select exactly $P - n$ individuals from P_{t-1} and copy them to a new population P_t .

Step 6 Select uniformly parents from M_t to produce exactly n offsprings (as in **GAR II**, but in this case the genetic operators act only on n individuals stored in the mating pool).

Step 7 Add new offsprings to population P_t .

3.3.7 Hybrid genetic algorithm (HGA)

GAs are generally very efficient in finding promising areas of the searched solution. On the other hand, they may perform rather poorly when shooting for the exact solution with a high degree of precision (premature convergence, convergence to a local minimum, etc.). Therefore it appears logical (see also discussion in Section 3.2.5) to combine GAs exploring the search space initially with a deterministic optimizer exploiting promising solutions locally.

As natural for GAs, this procedure can be implemented in a number of ways. When experimenting with this approach, various ideas suggested up to date were combined, which eventually led to a reliable and efficient algorithm. It works with relatively small population

sizes, which makes computationally feasible to restart the genetic algorithm after a given convergence criterion is met. Each restart is associated with a certain number of new members entering the initial population to maintain a sufficient diversity among chromosomes. Consequently, mutation operators can be excluded from reproduction. Individual steps of this algorithm are now discussed in a sequel:

Step 2 Randomly generate a small population.

Steps 5&6 Perform standard genetic operations until convergence or the maximum number of generations exceeded. To select chromosomes for reproduction *stochastic tournament selection* scheme is applied. Only crossover operators are used.

Step 7a Select n best individuals for local search. We adopt the *Dynamic Hill Climbing* method of Yuret (Section 3.2.2) to seek for the desired optimum with a starting point provided by the GA. When the local optimizer converges copy new individuals into P_t .

Step 7b Add $P - n$ randomly generated individuals to fill population P_t . This ensures diversity among chromosomes. Goto step 5 and restart the GA.

3.3.8 Differential evolution (DE)

Differential evolution is very simple stochastic optimization method proposed by Storn and Price [Storn and Price, 1995]. This method is reported to have very good results in various minimization problems [Storn, 1996].

To reveal its similarities and differences with previous algorithms the principle of this method will be demonstrated within the particular steps of Algorithm 3.4.¹

¹ In this work only one variant – called DE1 in [Storn and Price, 1995] – was tested. Interested reader can inspect <http://http.icsi.berkeley.edu/~storn> for additional variants of this method.

Step 2 The initial population should be spread as much as possible over the solution space \mathcal{S} . The size of the initial population should be $\approx 10D$, where D is the dimension of a problem.

Step 5 Individuals subjected to the operation are picked from population sequentially, no attention is paid to the value of their fitness.

Step 6 First, a new perturbed vector \mathbf{Y}' is generated according to

$$\mathbf{Y}' = \mathbf{X}^j + F(\mathbf{X}^k - \mathbf{X}^l),$$

where j, k, l are mutually different indexes, generated as integer random numbers with uniform distribution of interval $\langle 1; P \rangle$, F is the parameter of the method and superscripts refer to the position of an individual in the population. Then, this new individual is subjected to two-point crossover with starting point $n = u[1, D]$ and endpoint $(n + L)\%D$, where L is the length of the exchange interval and $\%$ stands for modulo, such that probability $Pr(L \geq n) = CR^{(n-1)}$, where crossover rate CR is the second user-defined parameter (see [Storn and Price, 1995] for more details). New individual is then given by:

$$x'_i = \begin{cases} y'_i & \text{for } i = n, \dots, (n + L - 1)\%D \\ x_i & \text{otherwise.} \end{cases}$$

Step 7 New individual is inserted into new population only if it is better in terms of fitness.

3.3.9 Augmented simulated annealing (AUSA)

When talking about stochastic optimization algorithms, it would be unfair not to mention another popular method using random choice to explore the solution space, namely the *Augmented simulated annealing method* presented by [Mahfoud and Goldberg, 1992]. This method effectively exploits the essentials of GAs (a population of chromosomes, rather than a single point in space, is optimized) together with the basic concept of simulated annealing method guiding the search towards minimum energy states.

If we wish to put GAs and the **AUSA** on the same footing, we may relate the **AUSA** to a group of *Steady state* and *On the fly* methods [[Michalewicz, 1992](#)], in which offspring replaces its parents immediately. The replacement procedure is controlled by the Metropolis criterion, which allows a worse child to replace its better parent with only a certain probability. The probability of accepting a worse solution is reduced as the procedure converges to the “global” minimum.

The following algorithm describes an implementation of the **AUSA**:

```

1   $T = T_{\max}, t = 0$ 
2  generate  $P_0$ , evaluate  $P_0$ 
3  while (not termination-condition) {
4       $counter = success = 0$ 
5      while(  $counter < counter_{\max} \wedge success < success_{\max}$  ) {
6           $counter = counter + 1, t = t + 1$ 
7          select operator  $O$ 
8          select individual(s)  $I_t$  from  $P_t$ 
9          modify  $I_t$  by  $O$ 
10         select individual(s)  $I'_t$  from  $P_t$ 
11          $p = \exp((F(I'_t) - F(I_t))/T)$ 
12         if ( $u(0, 1) \leq p$ ) {
13              $success = success + 1$ 
14             insert  $I_t$  into  $P_t$  instead of parents
15             evaluate  $P_t$ 
16         }
17     }
18     decrease  $T$ 
19 }
```

Algorithm 3.5: Augmented Simulated Annealing

Step 7 It is recommended to choose mutation operators with much higher probabilities than crossovers. In [Kvasnička, 1993] ratio ≈ 0.1 is proposed.

Step 8 New individuals are selected using the *normalized geometric ranking* method.

Step 11 The temperature T_{\max} should be chosen such that the ratio of accepted solutions to all solutions is $\approx 50\%$.

Step 18 This step is called the *cooling schedule*. We use a very simple form of cooling schedule $T_{i+1} = T_{\text{mult}}T_i$. In this step we also perform *reannealing* if necessary. If the actual temperature is lower than a given parameter T_{\min} , we set $T = T_{\max}$ and copy a half of the current population to a new one. Remaining part of a new population is generated randomly.

3.3.10 Test example

To test the performance of proposed methods the same problem as in Section 3.2.4 was considered. As in previous case, each algorithm was run independently 20 times with parameters given in Appendix B. Again, the minimum, maximum and average values of function evaluation and value of the objective function of the best chromosome in the population were recorded. Initial population was generated purely randomly in all runs.

Moreover, for all algorithms a simple procedure was implemented to maintain a sufficient diversity in a population. Before inserting an offspring \mathbf{X} into population, we first search for an individual \mathbf{X}' which satisfies

$$F(\mathbf{X}) = F(\mathbf{X}') \quad \max_i |x_i - x'_i| < \varepsilon, i = 1, \dots, 2N,$$

where ε is set here to 1×10^{-5} . If such an individual exists, it is replaced by \mathbf{X} . Otherwise an individual \mathbf{X} enters a population following step 7 of Algorithm 3.4.

Results and conclusions. As it is evident from Table 3.3, the results obtained by various genetic algorithms and by the augmented simulated annealing are substantially better than results obtained by deterministic algorithms and the method of differential evolution, which performs rather poorly for this particular example. From different versions of genetic algorithms only **GA I** was not able to find the value of objective function 6×10^{-5} two times.

Algorithm	Number	Returned value $\times 10^5$		
	found	Min	Avg	Max
GA I	18/20	6.0	7.2	16.4
GA II	20/20	5.9	6.0	6.0
GA III	20/20	5.9	6.0	6.0
DE	0/20	106.0	210.7	295.9
HGA	20/20	5.9	6.0	6.0
AUSA	20/20	5.9	6.0	6.0

Table 3.3: Characteristics of the best individual

It can be seen that the performance of algorithms **GA II**, **GA III**, **HGA** and **AUSA** are similar. But, from the point of view of function evaluation shown in Table 3.4 the **HGA** and **AUSA** algorithms are slightly better than the other ones.

Finally, it is interesting to compare the results of the **DHC** listed in Table 3.1 and the **HGA** given in Table 3.3. It is evident that combination of genetic algorithm with local optimizer is very advantageous - the algorithm was able to find the required value of the objective function 6×10^{-5} in all cases and the average number of function evaluations is approximately only 5% of the original value.

3.4 Some additional improvements

In this Section, we try to further improve the performance of the stochastic optimizers implementing more advanced techniques used for genetic algorithms. Particularly, the adaptive operator probabilities and incorporation of the problem-dependent information into the genetic operators are inspected.

Algorithm	Number of evaluations		
	Min	Avg	Max
GA I	8,896	74,562	193,600
GA II	6,956	17,270	55,296
GA III	4,484	12,037	26,224
DE	-	-	-
HGA	1,613	8,856	24,404
AUSA	3,490	8,709	26,314

Table 3.4: Number of function evaluations for stochastic optimizers

3.4.1 Adaptive operator probabilities

The one of the most difficult problems faced when using a stochastic algorithm is the proper setting of algorithms parameters. As shown in Appendix B, this task is far from trivial - eg. **AUSA** method needs to set up seventeen different parameters. Moreover, it is well known, that the role of different operators during the optimization run changes (see discussion in [Michalewicz et al., 1994] for current operators).

In [Davis, 1989], method for determination of adaptive operator probabilities was established. The key idea of his approach is that operators, which produce better offsprings should be used more often than those performing poorly. Further, besides rewarding the operator which produced the good offspring the operator responsible for creating the parent should be rewarded as well.

Let us briefly outline, how these informations are gathered. Whenever a new member is added to a population in step 7 of Algorithm 3.4 a pointer is set to its parent(s) and to the operator which created it. Further, a check is performed if the new individual is the best one in the current population. If yes, the amount that it is better is stored as a “local delta”. These information are stored in some “adaptation window” which contains last W inserted members with parents considered M generations back. Then, after each

I inserted new individuals, performance of each operator is computed. In the first step, every offspring in adaptation window passes P times its local delta to its parents and this parent(s) passes P portion of this value back to their parents etc. Then, delta is summed for all members in adaptation window for all operators and operator probabilities are updated - each operator keeps S portion of its original value and remaining part is redistributed according to operators performance. For more information see [Davis, 1989].

This procedure was used for the **AUSA** algorithm. As the first step, the initial operator probabilities were determined by the procedure suggested in [Davis, 1989] – initially, every operator was given the same probability and parameter S was set to 0.01. Then, the algorithm was run 20 times until the first adaptation took place. The adapted values from 20 runs were averaged to obtain the initial probabilities of various operators. The setting of adaptation parameters is given in Table B.8 and the resulting operator probabilities are displayed in Table 3.5. It is evident that for the initial parts of the optimization process most of the progress is done by the boundary mutation and simple arithmetic crossover.

<i>Operator</i>	<i>Initial probability</i>
Uniform mutation	0.150
Boundary mutation	0.278
Non-uniform mutation	0.063
Multi-non uniform mutation	0.048
Simple crossover	0.040
Simple arithmetic crossover	0.233
Whole arithmetic crossover	0.097
Heuristic crossover	0.088

Table 3.5: Initial operator probabilities resulting from adaptation procedure

Then, the algorithm was run 20 times using this initial values of operator probabilities. The adaptivity setting was the same as in the previous example, only value of S was set to .7.

Number found	Returned value $\times 10^5$			Number of evaluations		
	Min	Avg	Max	Min	Avg	Max
12/20	5.9	11.8	36.9	2,092	6,358	25,316

Table 3.6: AUSA algorithm with adaptive operator probabilities

Results of this test are shown in Table 3.6.

Unfortunately, this approach does not seem to be useful for our particular problem. The reason is obvious - the optimization procedure gets trapped in a local minimum. This is primarily caused by the fact, that during optimization run the probability of crossover operators gets higher and higher (because they produce good offspring) so the the diversity of population is quickly decreasing. On the other hand, if this algorithm succeeds in locating the required value, it is done more faster than for the stand alone algorithm.

3.4.2 Problem-dependent operators

It is no secret that the performance of genetic algorithms can be substantially improved by putting in use the knowledge of the problem nature for the chromosome coding or for developing the problem-specific operators (see [Beasley et al., 1993b, Michalewicz, 1992]). The latter approach is explored in this section.

Suppose that the parent configuration we selected for reproduction meets the *impenetrability constraint* imposed on the fibers arrangement. In the recombination step we wish to introduce only such operators, which yield an offspring configuration complying with the impenetrability condition as well. To state this in more formal manner, we define the search space as

$$\mathcal{S} = \left\{ x^i \in \langle 0; H_1 \rangle, y^i \in \langle 0; H_2 \rangle : \sqrt{(x^i - x^j)^2 + (y^i - y^j)^2} \geq 2R; i, j = 1, \dots, N \right\}. \quad (3.4)$$

The simplest way to fulfill the above condition may rely on randomly generating a vector \mathbf{x}' until the condition $\mathbf{x}' \in \mathcal{S}$ is met (death penalty to an infeasible individual (see eg.

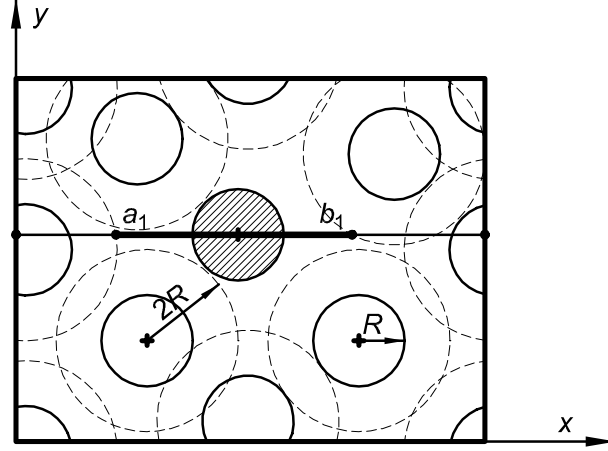


Figure 3.3: Allowable position of particle

[Povirk, 1995, Yeong and Torquato, 1998]). Clearly, this process may become prohibitively expensive, especially for a higher concentration of fibers.

To deal with this problem, it is more efficient to first determine a set of possible locations of all particles and successively generate a new particle or particles, which belong to this set. Unfortunately, solving this problem in its full generality is rather complicated. Thus, instead of identifying allowable locations of *all* particles, we limit our attention to a set of possible locations of *one particle* permitted to translate either in the x or y direction, while the coordinates of the remaining fibers are kept fixed. We shall denote these sets as

$$\begin{aligned}\mathcal{S}|_{y^i} &= \{x^i \in \langle 0; H_1 \rangle : \mathbf{x} \in \mathcal{S}\} \\ \mathcal{S}|_{x^i} &= \{y^i \in \langle 0; H_2 \rangle : \mathbf{x} \in \mathcal{S}\}.\end{aligned}\tag{3.5}$$

To construct the above sets imagine a collection of identical cylinders, surrounded by a certain concentric protective cylindrical surface with diameter equal to $2R$ (see also discussion in Section 2.2.2). In view of the impenetrability constraint the secure cylinder cannot be occupied by another fibers' center. In particular, to identify space $\mathcal{S}|_{y^i}$ with the i -th particle we draw a line $x = x^i$, which intersects the protective surfaces around all remaining fibers in $n - 1$ intervals $\langle a'_j; b'_j \rangle$ where $j = 1, \dots, (n - 1)$. Then the set $\mathcal{S}|_{y^i}$ of allowable locations

of the particle i is given by (see Fig 3.3)

$$\mathcal{S}|_{y^i} = \langle 0; H_1 \rangle \setminus \bigcup_{j=1}^{n-1} \langle a'_j; b'_j \rangle = \bigcup_{j=1}^n \langle a_j; b_j \rangle. \quad (3.6)$$

Similarly we write

$$\mathcal{S}|_{x^i} = \langle 0; H_2 \rangle \setminus \bigcup_{j=1}^{n-1} \langle a'_j; b'_j \rangle = \bigcup_{j=1}^n \langle a_j; b_j \rangle. \quad (3.7)$$

In the spirit of Eqs. (3.6) and (3.7) we can now define the following set of problem-specific operators (see also [Michalewicz et al., 1994]):

Uniform mutation Generate an integer number $i = u[1, N]$ with uniform distribution on a closed interval $\langle 1; N \rangle$, select the x or y coordinate, evaluate $\mathcal{S}|_{x^i}$ or $\mathcal{S}|_{y^i}$, select $k = u[1, n]$ and set:

$$x'^i = x^i + u(a_k, b_k)$$

or

$$y'^i = y^i + u(a_k, b_k),$$

while fixing the remaining coordinates.

Non-uniform mutation Select $i = u[1, N]$ and the x or y coordinate, evaluate $\mathcal{S}|_{x^i}$ or $\mathcal{S}|_{y^i}$. Select k such that $x^i \in \langle a_k; b_k \rangle$ or $y^i \in \langle a_k; b_k \rangle$, generate a real number $p = u(0, 1)$ with uniform distribution on a closed interval $\langle 0; 1 \rangle$ and set:

$$x'_i = \begin{cases} x^i + (b_k - x^i)f(t), & \text{if } p < .5 \\ x^i + (a_k - x^i)f(t), & \text{if } p \geq .5 \end{cases}$$

or

$$y'_i = \begin{cases} y^i + (b^k - y^i)f(t), & \text{if } p < .5 \\ y^i + (a^k - y^i)f(t), & \text{if } p \geq .5 \end{cases},$$

while fixing the remaining coordinates. The number $f(t)$ is the same as in Section 3.3.3.

Multi-non-uniform mutation Non-uniform mutation applied successively to all coordinates of \mathbf{X} .

Simple two-point crossover Select $i = u[1, n]$ and $j = u[1, n] \wedge i < j$. Repeat for $k = i, \dots, j$:

$$\begin{aligned} {}^1x'^k &= {}^1x^k(1 - \alpha) + {}^2x^k\alpha \\ {}^2x'^k &= {}^1x^k\alpha + {}^2x^k(1 - \alpha), \end{aligned}$$

and

$$\begin{aligned} {}^1y'^k &= {}^1y^k(1 - \alpha) + {}^2y^k\alpha \\ {}^2y'^k &= {}^1y^k\alpha + {}^2y^k(1 - \alpha), \end{aligned}$$

where eg. ${}^2x^k$ corresponds to the x coordinate of k -th particles of the second parent. The parameter α is set to 1 initially. If $x'^k \notin \mathcal{S}|_{y^i}$ or $y'^k \notin \mathcal{S}|_{x^i}$ respectively, decrease α by $1/n_d$; n_d is the user-defined parameter (number of decreasing steps). This procedure is repeated until $x'^k \in \mathcal{S}|_{y^i}$ or $y'^k \in \mathcal{S}|_{x^i}$ holds (this condition is always met for $\alpha = 0$).

These operators were implemented to **AUSA** algorithm and the proof test was run again. Initial population consisted of non-penetrable particles. Parameters of the method are given in Appendix B. Results in Table 3.7 show, that this approach is very efficient since the required value of the objective function was found for all 20 runs and the average number of evaluations was reduced by 50%.

Number found	Returned value $\times 10^5$			Number of evaluations		
	Min	Avg	Max	Min	Avg	Max
20/20	5.9	6.0	6.0	543	4,403	11,516

Table 3.7: AUSA algorithm with problem-dependent operators

3.4.3 Sampling grid refinement

To check the quality of the resultant unit cell let us plot the second order intensity function for the original microstructure ($K_0(r)$) against the one associated with a unit cell chosen

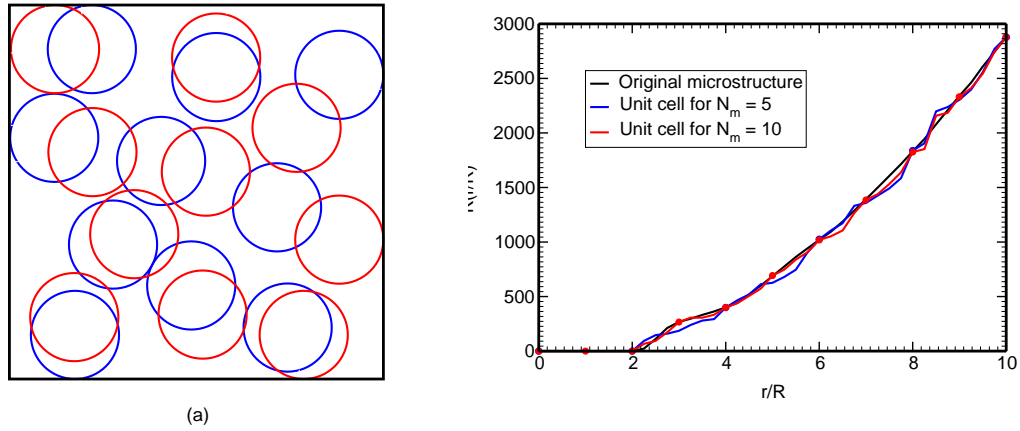


Figure 3.4: Periodic unit cells with corresponding second order intensity functions

as the minimum from 20 independent runs. Results, which appear in Fig. 3.4(b), were again derived via the **AUSA** method. Evidently, both functions agree well at sampled points. Unfortunately, a significant deviation is distinct in all other points. To improve coincidence of both curves the number of sampled points N_m must be increased. Fig. 3.4 shows results of such procedure. It is interesting to note that when running for example the **AUSA** for $N_m = 10$ from the beginning, we arrived at the minimum equal to 1.63×10^{-4} after approximately 173,000 function evaluations. However, when starting with $N_m = 5$ and then continuing with $N_m = 10$ we received the desired minimum after 115,000 function evaluations only. Thus, using the results obtained for coarser grid of sampling points as a initial population for foregoing optimization can save large amount of function evaluations.

3.5 Determination of periodic unit cell

In this Section, method used for the determination of a periodic unit cell is described in more details. Results obtained by this procedure are demonstrated and discussed.

Finding optimal fiber configuration. Optimal fiber configuration was determined by the **AUSA** method (Algorithm 3.5) with the problem-specific operators (see Section

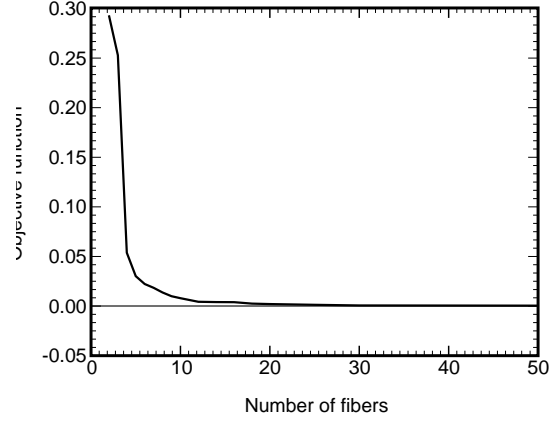


Figure 3.5: Variation of the objective function with the number of particles in the PUC.

3.4.2). Parameter settings are given in Appendix B, Table B.9. Optimization was first performed only for $N_m = 4$ with fibers spaced by one fiber diameter. Then, value of N_m was raised to 8,16,24 and 32. Sampled points were biased towards the value of $r = 2R$ in order to capture an apparent correlation of individual space points within the sample. Best 50% of individuals were copied into new population to provide good initial guesses for subsequent optimization.

Termination conditions. For each value of N_m , iteration was terminated when one of the following conditions was met:

- Algorithm returned value $F(\mathbf{x}^N, H_1, H_2) < \varepsilon = 10^{-4}$.
- Number of function evaluation exceeded 250,000.

The first condition is usually fulfilled for small values of N_m , while the second one takes effect in remaining cases. As the value of the objective function $F(\mathbf{x}^N, H_1, H_2)$ for given H_1 and H_2 the result obtained for $N_m = 32$ was used.

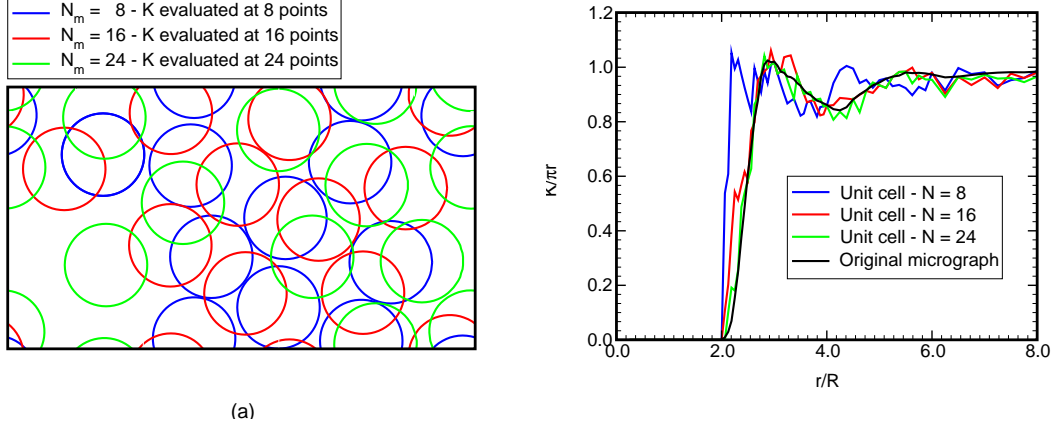


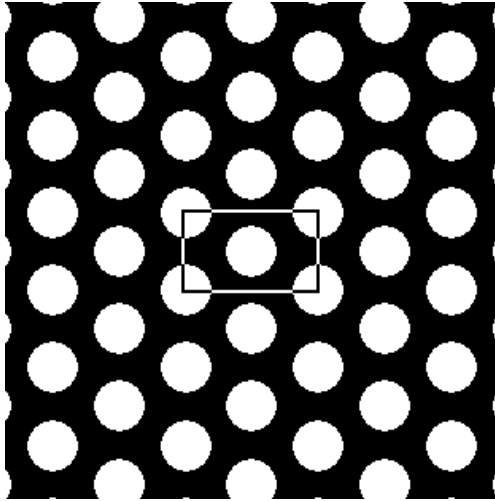
Figure 3.6: Evolution of the 10 particles PUC

Finding the optimal side ratio. This step was performed by Golden Section search method (Algorithm 3.1) with values $\eta_a = 1.0$, $\eta_b = 2.0$ and $\epsilon = .05$.

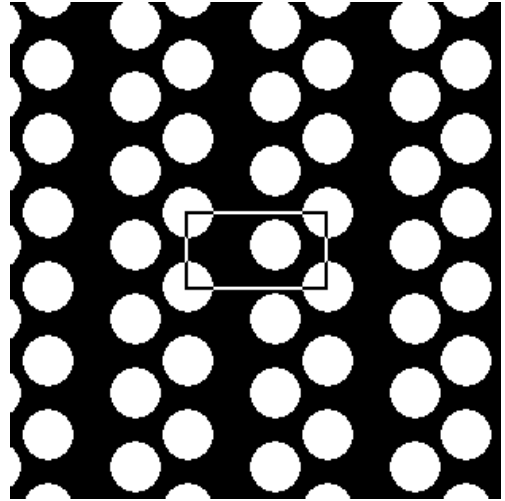
Results for a different number of particles within the unit cell are shown in Fig. 3.5. Values of objective function are relatively high, eg. the value of objective function lesser than 10^{-2} is firstly reached for 10-fiber periodic unit cell. To explain this fact, let us consider the results obtained for the periodic unit cell with 10 particles (Fig. 3.6). Evolution of the unit cell with increasing accuracy of the solution is plotted in Fig. 3.6(a), whereas Fig. 3.6(b) displays a variation of the normalized second order intensity function $K(r)/\pi r^2$ corresponding to various stages of the solution process. From this Figure, two facts are evident – first : for all values of N_m it is clear, that there is the jump of the objective function located at r corresponding to side length of unit cell, which results in quite large deviation of these two functions. Secondly, function corresponding to the periodic media agrees well in sampled points but in the neighboring points is quite noisy. This is probably caused by the relatively small number of particles in the unit cell comparing to the original microstructure. Nevertheless, to judge the quality of unit cells one should take into account the effective behavior of resultant periodic composite material rather than measuring the

quality of obtained unit cells by an artificially defined objective function. This is the objective of following Chapter.

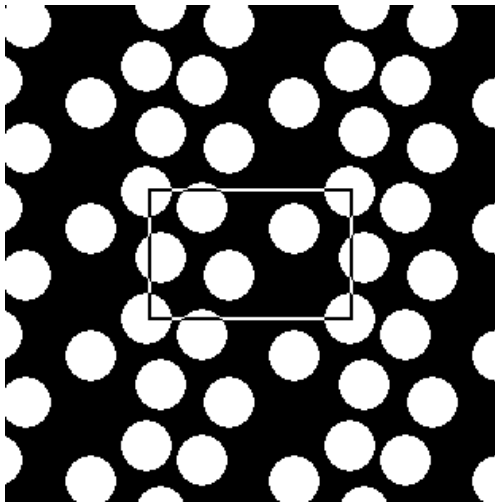
Finally, some examples of the resulting unit cells are given in Fig. 3.7 together with the hexagonal lattice shown for comparison. It is evident, that periodic unit cells resulting from optimization capture the clustering of particles in the original micrograph to some extent.



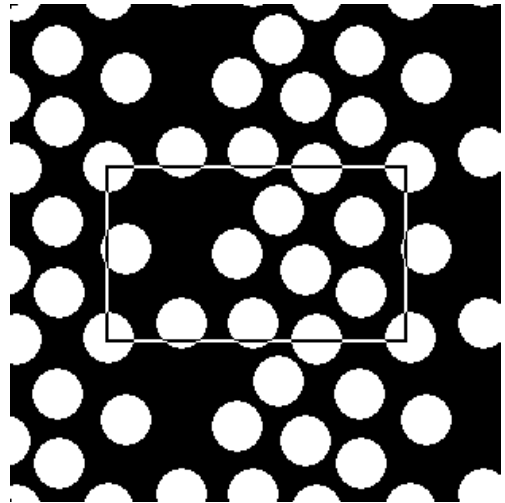
(a)



(b)



(c)



(d)

Figure 3.7: Periodic unit cells: (a) Hexagonal lattice, (b) 2-fibers PUC, (c) 5-fibers PUC, (d) 10-fibers PUC.

Chapter 4

EFFECTIVE PROPERTIES OF PERIODIC COMPOSITE MEDIUM

This Chapter is devoted to the testing of resultant periodic unit cells obtained by optimization procedure in Chapter 3 from the effective elastic behavior point of view. The effective elastic properties of the material formed by the periodic unit cell are obtained by the Finite Element Method and compared with results provided by the Mori-Tanaka method and by the periodic unit cell with hexagonal arrangement of fibers.

Section 4.1 outlines basic relation pertinent to evaluation of the effective elastic properties of unidirectional composites. Then, in Section 4.2 and 4.3 two specific procedures determining the effective properties – namely the Mori-Tanaka method and numerical procedure based on the Finite Element analysis – are discussed. Finally, Section 4.4 shows various numerical results obtained for different periodic unit cells.

4.1 *Basic relations*

A common approach when dealing with composite structures is to replace their inhomogeneous microstructure with some *homogenized* or *effective* material which exhibits the same overall behavior as the non-homogeneous one. Since in this work only the elastic behavior of the composite material is considered, the homogenized medium is uniquely characterized by its effective material stiffness or compliance tensor.

The elastic behavior of such a material is determined by displacement, strain and stress fields given by

$$\epsilon_{ij}(\mathbf{x}) = \frac{1}{2} \left(\frac{\partial u_i(\mathbf{x})}{\partial x_j} + \frac{\partial u_j(\mathbf{x})}{\partial x_i} \right), \quad (4.1)$$

$$\sigma_{ij}(\mathbf{x}) = L_{ijkl}(\mathbf{x}) : \epsilon_{kl}(\mathbf{x}),$$

$$\epsilon_{ij}(\mathbf{x}) = M_{ijkl}(\mathbf{x}) : \sigma_{kl}(\mathbf{x}), \quad (4.2)$$

$$\frac{\partial \sigma_{ij}(\mathbf{x})}{\partial x_j} = f_i(\mathbf{x}), \quad (4.3)$$

where u_i is the displacement field, ϵ_{ij} and σ_{ij} stand for the strain and stress field, L_{ijkl} is the tensor of material stiffness, M_{ijkl} is the tensor of material compliance such that $L_{ijkl}^{-1} = M_{ijkl}$ and f_i is the vector of body forces.

When analyzing the unidirectional fiber composite systems it is usually sufficient to use the *generalized plane strain* conditions. In such a state, the only non-zero components of strain and stress tensors are $\epsilon_{11}, \epsilon_{12}, \epsilon_{22}, \epsilon_{33}$ and $\sigma_{11}, \sigma_{12}, \sigma_{22}, \sigma_{33}$ respectively. Note that due to perfect bonding between individual phases components ϵ_{33} and σ_{33} attain constant values. Employing Hill's notation [Hill, 1964] the material stiffness tensor assumes the form

$$\mathbf{L} = \begin{bmatrix} (k+m) & (k-m) & 0 & l \\ (k-m) & (k+m) & 0 & l \\ 0 & 0 & m & 0 \\ l & l & 0 & n \end{bmatrix}, \quad (4.4)$$

where constants k, m, n and l are connected with material engineering constants by

$$\begin{aligned} k &= -[1/G_T - 4/E_T + 4\nu_A^2/E_A]^{-1} & l &= 2k\nu_A \\ n &= E_A + 4k\nu_A^2 & m &= G_T. \end{aligned}$$

Then, to determine the *effective* properties of homogenized media one should relate the average stress and strain fields in the spirit of Eq. (4.2). Thus, prescribing average strain to be $\langle \epsilon(\mathbf{x}) \rangle = \epsilon_0$ or average stress to be $\langle \sigma(\mathbf{x}) \rangle = \sigma_0$, the effective characteristics of composite

media are provided by:

$$\langle \boldsymbol{\sigma}(\mathbf{x}) \rangle = \langle \mathbf{L}(\mathbf{x}) : \boldsymbol{\epsilon}(\mathbf{x}) \rangle = \mathbf{L} : \boldsymbol{\epsilon}_0, \quad (4.5)$$

$$\langle \boldsymbol{\epsilon}(\mathbf{x}) \rangle = \langle \mathbf{M}(\mathbf{x}) : \boldsymbol{\sigma}(\mathbf{x}) \rangle = \mathbf{M} : \boldsymbol{\sigma}_0, \quad (4.6)$$

where $\langle \cdot \rangle$ stands for spatial average of particular field and \mathbf{L} and \mathbf{M} are the effective stiffness and compliance tensors of the heterogenous material.

4.1.1 Hill's lemma

The principal step when determining the effective properties is provided by *Hill's relation*. He proved that for compatible strain and equilibrated stress fields the following relation holds [Hill, 1963]:

$$\langle \boldsymbol{\sigma}(\mathbf{x}) : \boldsymbol{\epsilon}(\mathbf{x}) \rangle = \langle \boldsymbol{\sigma}(\mathbf{x}) \rangle : \langle \boldsymbol{\epsilon}(\mathbf{x}) \rangle. \quad (4.7)$$

This relation in fact states that the average of “microscopic” internal work is equal to the macroscopic work done by internal forces.

Then, again prescribing the average strain $\langle \boldsymbol{\epsilon}(\mathbf{x}) \rangle = \boldsymbol{\epsilon}_0$ or average stress $\langle \boldsymbol{\sigma}(\mathbf{x}) \rangle = \boldsymbol{\sigma}_0$, the effective properties can be alternatively defined using Eqs. (4.5,4.6) as

$$\boldsymbol{\epsilon}_0 : \mathbf{L} : \boldsymbol{\epsilon}_0 = \langle \boldsymbol{\epsilon}(\mathbf{x}) : \mathbf{L}(\mathbf{x}) : \boldsymbol{\epsilon}(\mathbf{x}) \rangle, \quad (4.8)$$

$$\boldsymbol{\sigma}_0 : \mathbf{M} : \boldsymbol{\sigma}_0 = \langle \boldsymbol{\sigma}(\mathbf{x}) : \mathbf{M}(\mathbf{x}) : \boldsymbol{\sigma}(\mathbf{x}) \rangle. \quad (4.9)$$

4.1.2 Stress and strain concentration factors

Sometimes, it is convenient to establish the connection between average stresses and strains for given phases and overall prescribed values of stress or strain by [Hill, 1963]:

$$\boldsymbol{\epsilon}_r = \mathbf{A}_r : \boldsymbol{\epsilon}_0, \quad (4.10)$$

$$\boldsymbol{\sigma}_r = \mathbf{B}_r : \boldsymbol{\sigma}_0, \quad (4.11)$$

where \mathbf{A}_r and \mathbf{B}_r are stress and strain concentration factors of r -th phase, $\boldsymbol{\epsilon}_r$ and $\boldsymbol{\sigma}_r$ stands for the average value of stress and strain values in the r -th phase, $r = f, m$. Noticing that

$$\boldsymbol{\epsilon}_0 = c_m \boldsymbol{\epsilon}_m + c_f \boldsymbol{\epsilon}_f, \quad (4.12)$$

$$\boldsymbol{\sigma}_0 = c_m \boldsymbol{\sigma}_m + c_f \boldsymbol{\sigma}_f, \quad (4.13)$$

following relations can be established for individual concentration tensors of a two-phase media:

$$c_m \mathbf{A}_m + c_f \mathbf{A}_f = \mathbf{I}, \quad (4.14)$$

$$c_m \mathbf{B}_m + c_f \mathbf{B}_f = \mathbf{I}. \quad (4.15)$$

Thus, once the concentration factor for one phase is known it is possible to express the concentration factor for the second phase.

Finally, recognizing that $\boldsymbol{\sigma}_r = \mathbf{L}_r \boldsymbol{\epsilon}_r$ and $\boldsymbol{\epsilon}_r = \mathbf{M}_r \boldsymbol{\sigma}_r$, the effective material properties can be expressed as

$$\mathbf{L} = c_m \mathbf{A}_m \mathbf{L}_m + c_f \mathbf{A}_f \mathbf{L}_f, \quad (4.16)$$

$$\mathbf{M} = c_m \mathbf{B}_m \mathbf{M}_m + c_f \mathbf{B}_f \mathbf{M}_f. \quad (4.17)$$

4.2 Mori-Tanaka method

Let us consider the isolated fiber embedded in the infinite matrix subjected to far-field load σ_0 . It follows from work of Eshelby [Eshelby, 1957], that stress field inside the fiber is constant and can be uniquely determined by values of \mathbf{L}_m , \mathbf{L}_f and Eshelby's tensor \mathbf{S} . In the reformulation of Mori-Tanaka method by Benveniste [Benveniste, 1987], the isolated inclusion is loaded by average stress in matrix. Then, stress inside the fiber is provided by

$$\boldsymbol{\sigma}_f = \mathbf{W}_f \boldsymbol{\sigma}_m, \quad (4.18)$$

where \mathbf{W}_f is partial concentration factor is given by

$$\mathbf{W}_f = \mathbf{L}_f \left[\mathbf{I} + \mathbf{S} \mathbf{L}_m^{-1} (\mathbf{L}_f - \mathbf{L}_m) \right]^{-1} \mathbf{L}_m^{-1}. \quad (4.19)$$

The tensor \mathbf{S} can be expressed via polarization tensor \mathbf{P} as $\mathbf{P} = \mathbf{S}\mathbf{L}_m^{-1}$, which for cylindrical fibers assumes the form [Sejnoha, 1999]:

$$\begin{aligned} P_{22} = P_{33} &= \frac{k_m + 4m_m}{8m_m(k_m + m_m)} & P_{23} = P_{32} &= \frac{-k_m}{8m_m(k_m + m_m)} \\ P_{44} &= \frac{k_m + 2m_m}{2m_m(k_m + m_m)} & P_{55} = P_{66} &= 1/(2p_m), \end{aligned} \quad (4.20)$$

where indexes of \mathbf{P} correspond to engineering notation (see eg. [Bittnar and Šejnoha, 1992]). The total stress concentration factors with help of Eq. (4.13) are obtained by

$$\mathbf{B}_f = \mathbf{W}_f(c_m\mathbf{I} + c_f\mathbf{W}_f)^{-1} \quad \mathbf{B}_m = (c_m\mathbf{I} + c_f\mathbf{W}_f)^{-1}. \quad (4.21)$$

Therefore, using Eq. (4.17), effective compliance material tensor yields

$$\mathbf{M} = [c_m\mathbf{M}_f\mathbf{W}_f + c_m\mathbf{M}_m](c_m\mathbf{I} + c_f\mathbf{W}_f)^{-1}. \quad (4.22)$$

Finally, effective stiffness tensor then can be obtained as $\mathbf{L} = \mathbf{M}^{-1}$.

4.3 Finite element formulation

When employing the Finite Element Method it is very advantageous to exploit the periodicity of the media. Since the microstructure of composite media is periodic with period Ω (periodic unit cell), the stress and strain field as well as material characteristics appearing in Eqs. (4.1–4.3) are periodic as well. Let us suppose that our unit cell is loaded by prescribed value of ϵ_0 . For foregoing analysis it is convenient to split the field $\mathbf{u}(\mathbf{x})$ into periodic part and part corresponding to overall strain in the form

$$\mathbf{u}(\mathbf{x}) = \epsilon_0 \cdot \mathbf{x} + \mathbf{u}^*(\mathbf{x}), \quad (4.23)$$

where the first term in previous equation corresponds to affine displacement due to prescribed uniform strain ϵ_0 [Michel et al., 1999] and second term is the Ω -periodic part of $\mathbf{u}(\mathbf{x})$. Once $\mathbf{u}^*(\mathbf{x})$ is known, stress and strain field are given by

$$\epsilon(\mathbf{x}) = \epsilon_0 + \epsilon^*(\mathbf{x}), \quad (4.24)$$

$$\sigma(\mathbf{x}) = \mathbf{L}(\mathbf{x}) : \epsilon(\mathbf{x}), \quad (4.25)$$

where $\boldsymbol{\epsilon}^*(\mathbf{x})$ represents here the fluctuating part of the strain field, which vanishes upon volume averaging.

To find the \mathbf{u}^* the *principle of minimum potential energy* [Bittnar and Šejnoha, 1992] is usually employed. This yields

$$\begin{aligned} 2 \langle W(\boldsymbol{\epsilon}(\mathbf{x})) \rangle &= \langle \boldsymbol{\epsilon}(\mathbf{u}(\mathbf{x})) : \mathbf{L}(\mathbf{x}) : \boldsymbol{\epsilon}(\mathbf{u}(\mathbf{x})) \rangle = \langle \boldsymbol{\epsilon}(\mathbf{u}(\mathbf{x})) \rangle : \langle \mathbf{L}(\mathbf{x}) : \boldsymbol{\epsilon}(\mathbf{u}(\mathbf{x})) \rangle \leq \\ &\leq \langle \boldsymbol{\epsilon}(\mathbf{v}(\mathbf{x})) \rangle : \langle \mathbf{L}(\mathbf{x}) : \boldsymbol{\epsilon}(\mathbf{v}(\mathbf{x})) \rangle, \end{aligned} \quad (4.26)$$

where $W(\cdot)$ represents the potential energy of the system for given strain field, \mathbf{v} is any kinematically admissible displacement field in the form $\mathbf{v}(\mathbf{x}) = \boldsymbol{\epsilon}_0 \cdot \mathbf{x} + \mathbf{v}^*$ and $\mathbf{v}^*(\mathbf{x})$ again corresponds to Ω -periodic fluctuating part of displacement field \mathbf{v} .

From this point, standard displacement-based Finite Element procedure can be employed [Bittnar and Šejnoha, 1992]. We start with the discretization of \mathbf{u} ,

$$\mathbf{u}(\mathbf{x}) = \boldsymbol{\epsilon}_0 \mathbf{x} + \mathbf{N}(\mathbf{x}) \mathbf{r}, \quad (4.27)$$

where $\mathbf{N}(\mathbf{x})$ stands for matrix of basis functions and \mathbf{r} is the vector of unknown degrees of freedom. Then, the strain field is provided by

$$\boldsymbol{\epsilon}(\mathbf{x}) = \boldsymbol{\epsilon}_0 + \mathbf{B}(\mathbf{x}) \mathbf{r}. \quad (4.28)$$

Minimization of Eq. (4.26) with respect to \mathbf{r} finally yields the system of equilibrium equations

$$\mathbf{K} \mathbf{r} = \mathbf{f}, \quad (4.29)$$

where

$$\begin{aligned} \mathbf{K} &= \sum_e \mathbf{K}^e \quad \text{where} \quad \mathbf{K}^e = \frac{1}{\Omega} \int_{A^e} \mathbf{B}^T \mathbf{L}^e \mathbf{B} \, dA^e \\ \mathbf{f} &= \sum_e \mathbf{f}^e \quad \text{where} \quad \mathbf{f}^e = -\frac{1}{\Omega} \int_{A^e} \mathbf{B}^T \mathbf{L}^e \boldsymbol{\epsilon}_0 \, dA^e, \end{aligned} \quad (4.30)$$

where \mathbf{K} is the stiffness matrix of the system, \mathbf{f} is a vector of global nodal forces resulting from the loading by $\boldsymbol{\epsilon}_0$, e stands for number of elements, A^e is the area of element e and Ω is the area of periodic unit cell.

Solution of this system of equation determines the \mathbf{u}^* up to the rigid body motion, which must be restricted by imposing appropriate boundary conditions. Due to the periodicity of the microstructure, these supports can be provided by fixing the corners of the unit cell. The second problem is implementing the periodicity condition on \mathbf{r} . A large number of approaches can be adopted to take this restriction into account (see [Michel et al., 1999] for details). In this work, this condition was simply fulfilled by assigning same code numbers to corresponding degrees of freedom related to the nodes on opposite sides of the unit cell.

To obtain the effective stiffness tensor, the periodic unit cell is successively loaded by strain fields ϵ_0 , which have one component equal to 1 and other 0. Performing the preceding procedure, one may find corresponding value of \mathbf{u}^* and determine $\langle \boldsymbol{\sigma}(\mathbf{x}) \rangle$. This value then corresponds to one row of the elastic stiffness tensor \mathbf{L} . By this algorithm, all components of the effective stiffness tensor can be obtained.

4.4 Numerical results

The aforementioned procedure was applied to equivalent unit cells resulting from optimization procedure as well as to the original sample displayed in Fig 2.6. Each of micrographs was discretized using CST triangle elements, the corresponding FEM meshes displayed in Fig 4.1 were created by **Triangle 1.3**¹ program. Finally, Table 4.1 shows the considered material properties of the matrix and fiber.

<i>Phase</i>	E_A	E_T	G_T	ν_A
	[GPa]	[GPa]	[GPa]	
Fiber	386	7.6	2.6	0.41
Matrix	5.5	5.5	1.96	0.40

Table 4.1: Material properties of T30/Epoxy system

¹ This program was obtained from <http://www.cs.cmu.edu/~quake/triangle.html>.

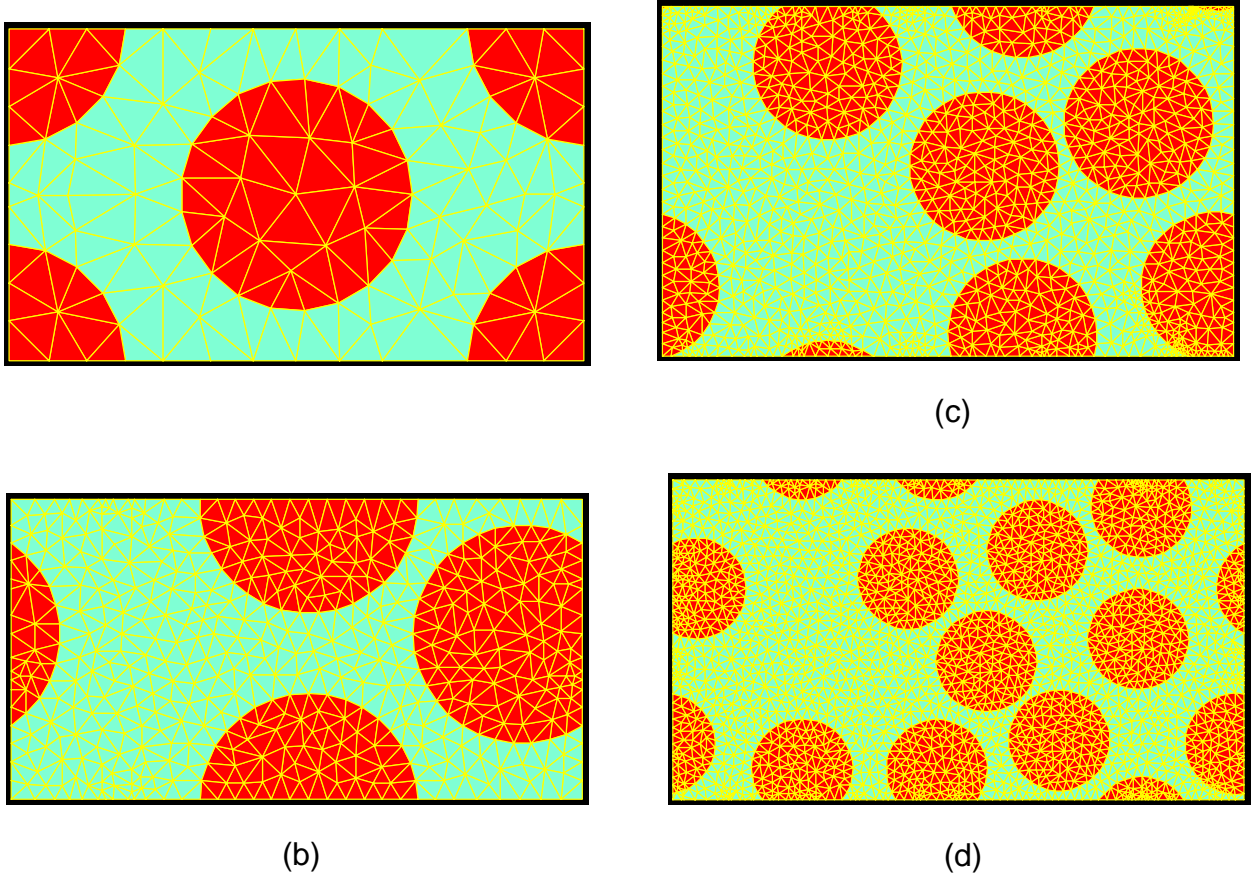


Figure 4.1: Example of Finite Element meshes: (a) Hexagonal lattice, (b) 2-fibers PUC, (c) 5-fibers PUC, (d) 10-fibers PUC.

First, to prove the applicability of the proposed method, the elastic moduli derived for the original microstructure, Fig 2.6, are compared with those found for the periodic unit cells displayed in Fig. 3.7. Selected components of the effective stiffness matrix \mathbf{L} are stored in Table 4.2. Results obtained for the hexagonal arrangements of fibers and found by the Mori-Tanaka method are provided for additional comparison. Evidently, the effective elastic properties obtained for the periodic unit cell, unlike those found by the hexagonal lattice and the Mori-Tanaka method, which correspond to the transversally isotropic medium, are capable to capture a slight anisotropy associated with the real microstructure. In addition, the results in Table 4.2 also promote the PUC consisting of 5 fibers only as the smallest one

<i>Unit cell</i>	L_{11}	L_{22}	L_{33}	L_{44}	c_f
Original	10.76	10.73	2.215	177.2	0.44
2 fibers PUC	10.78	10.75	2.202	177.2	0.44
5 fibers PUC	10.76	10.73	2.215	177.2	0.44
10 fibers PUC	10.76	10.73	2.215	177.2	0.44
Hexagonal array	10.74	10.74	2.213	177.3	0.44
Mori-Tanaka method	10.74	10.74	2.216	177.3	0.44

Table 4.2: Components of the effective stiffness matrix

we should consider for evaluation of the effective elastic material properties. Recall that the smallest number of fibers providing the reasonable value of objective function F in Chapter 3 was established to be 10.

To confirm our theoretical expectations, we investigated an influence of the proposed optimization technique on the effective moduli computed for the 10-fibers PUC derived from five independent optimization runs. As shown in Fig 3.6, the periodic unit cell substantially changes during the optimization run; moreover the resulting fiber configurations are not identical in different optimization runs. Nevertheless, results stored in Table 4.3 show that

<i>Modulus</i>	<i>Mean value</i>	<i>Standard deviation</i>	<i>Variation coefficient</i>
	[GPa]	[GPa]	[%]
L_{11}	10.76	0.013	0.12
L_{22}	10.73	0.013	0.12
L_{33}	2.215	0.003	0.13

Table 4.3: Variation of effective stiffness tensor for five ten-particle PUC resulting from optimization

<i>Modulus</i>	<i>Mean value</i>	<i>Standard deviation</i>	<i>Variation coefficient</i>
	[GPa]	[GPa]	[%]
L_{11}	10.73	0.32	2.97
L_{22}	10.71	0.38	3.54
L_{33}	2.210	0.07	3.48

Table 4.4: Variation of effective stiffness tensor for five randomly picked ten-particle PUC

the final moduli are not sensible to the particular fiber configuration (each optimization run provides a slight different fiber arrangements having, however, the same materials statistics up to the two-point probability function).

Finally, to support the present approach, the mean value and standard deviation of effective stiffnesses derived from five independent runs for unit cells defined through a random cut of the original micrograph Fig. 2.6 was found. Dimensions of such a unit cell were selected as to comply with dimensions found for the PUC consisting of 10 particles. Results given in Table 4.4 show that the differences in the moduli are not severe, however the variation coefficient is by orders of magnitude higher than for unit cells derived from the optimization procedure.

Chapter 5

CONCLUSIONS AND FUTURE WORK

A simple and intuitive approach based on microstructural statistics was proposed to determine periodic unit cells. This procedure was applied to the analysis of real composite material represented here by a bundle of graphite fibers surrounded by an epoxy matrix.

In Chapter 2 two different approaches suitable for the description of a unidirectional fiber composite microstructure were introduced. For each approach, the detailed discussion on microstructural characteristics up to the two-point level was presented together with the methods for their determination. Then, the validity of statistical isotropy and ergodicity assumptions for the composite material microstructure were confirmed by series of tests. These results allowed us to use the second order intensity function as a basic statistical descriptor in subsequent numerical computations.

Chapter 3 was concerned with the generation of the unit cell with the same statistics (up to two-point level) as possessed by the real microstructure. First, the objective function describing the similarity of the original material and the material formed by the periodic unit cell was defined in terms of the second order intensity function. Optimal geometrical arrangement of fibers within the periodic unit cell was then determined by minimizing the proposed objective function. The optimization procedure itself was performed in two stages - the Augmented Simulated Annealing method with problem-suited operators was found to be the most efficient tool for determination of the optimal fiber configuration, while dimensions of the unit cell were found by the Golden Section search method. It is worth to note, that the second order intensity function, although evaluated under the assumption of statistical isotropy, can capture clustering character of the real microstructure.

The effective properties of the material formed by the periodic unit cell and original

material were obtained by the Finite Element Method in Chapter 4 and compared with results provided by the Mori-Tanaka method and unit cell with hexagonal arrangement of fibers. Results show, that the corresponding periodic unit cells exhibit the slight anisotropy possessed by the original material. Further, the invariance of effective properties of unit cells resulting from different optimization runs was verified. However, although the resulting effective properties are not far from those corresponding to the hexagonal packing of fibers, an appreciable difference may appear when the contrast between the phases (ratio between the transverse Young's of the harder phase to the transverse Young's modulus of the softer phase) increases.

As shown in Chapter 4, the replacement of the complex material microstructure of the real material by the substantially simpler periodic unit cell is very convenient from the point of view of numerical determination of the material behavior. This approach can be extremely useful when examining the inelastic response of the composite material such as plasticity, debonding or damage and may provide useful insight into the effective behavior of composite materials. Moreover, since the microstructural characteristics are known for a given composite media, results obtained by numerical procedure can be compared with rigorous bound and estimates found when considering inelastic behavior of the material. These topics will be subjects of further investigation.

BIBLIOGRAPHY

- [Aboudi, 1991] Aboudi, J. (1991). *Mechanics of composite materials : A unified micromechanical approach*, volume 29 of *Studies in Applied Mechanics*. Elsevier.
- [Axelsen, 1995] Axelsen, M. (1995). *Quantitative description of the morphology and microdamage of composite materials*. PhD thesis, Aalborg University. Also available as <http://cwis.auc.dk/phd/fulltext/axelsen/pdf/axelsen.pdf>.
- [Baker, 1987] Baker, J. E. (1987). Reducing bias and inefficiency in the selection algorithm. In Grefenstette, J., editor, *Proceedings of the First International Conference on Genetic Algorithms*, pages 101–111. Lawrence Erlbaum Associates.
- [Beasley et al., 1993a] Beasley, D., Bull, D., and Martin, R. (1993a). An overview of Genetic Algorithms: Part 1, Foundations. *University Computing*, 15(2):58–69. Also available as ftp://ralph.cs.cf.ac.uk/pub/papers/GAs/ga_overview1.ps.
- [Beasley et al., 1993b] Beasley, D., Bull, D., and Martin, R. (1993b). An overview of Genetic Algorithms: Part 2, Research topics. *University Computing*, 15(4):17–69. Also available as ftp://ralph.cs.cf.ac.uk/pub/papers/GAs/ga_overview2.ps.
- [Benveniste, 1987] Benveniste, Y. (1987). A new approach to the application of Mori-Tanaka theory in composite materials. *Mechanics of Materials*, 6:147–157.
- [Beran, 1968] Beran, M. J. (1968). *Statistical Continuum Theories*. Monographs in Statistical Physics. Interscience Publishers.
- [Berryman, 1984] Berryman, J. G. (1984). Measurement of spatial correlation functions using image processing techniques. *Journal of Applied Physics*, 57(7):2374–2384.

- [Bittnar and Šejnoha, 1992] Bittnar, Z. and Šejnoha, J. (1992). *Numerické metody mechaniky*, volume 1. ČVUT.
- [Boublík, 1996] Boublík, T. (1996). *Statistická termodynamika*. Academia.
- [Burden and Faires, 1989] Burden, R. and Faires, J. D. (1989). *Numerical Analysis*. PWS-Kent Publishing Company, 4th edition.
- [Cerny, 1985] Cerny, J. (1985). Thermodynamical approach to the traveling salesman problem: An efficient simulation algorithm. *J. Opt. Theory Appl.*, 45:41–51.
- [Corson, 1974] Corson, P. B. (1974). Correlation functions for predicting properties of heterogeneous materials. I. Experimental measurement of spatial correlation functions in multiphase solids. *Journal of Applied Physics*, 45(7):3159–3164.
- [Davis, 1989] Davis, L. (1989). Adapting operator probabilities in genetic algorithm. In Schaffer, J. D., editor, *Proceeding of the Third International Conference on Genetic Algorithms*, pages 61–69. Morgan Kaufmann.
- [Drugan and Willis, 1996] Drugan, W. and Willis, J. (1996). A micromechanics-based non-local constitutive equation and estimates of representative volume element size for elastic composites. *Journal of the Mechanics and Physics of Solids*, 44(4):497–524.
- [Eshelby, 1957] Eshelby, J. D. (1957). The determination of the elastic field of an ellipsoidal inclusion and related problems. *Proceeding of Royal Society, Series A*, 241:376–396.
- [Gibson, 1994] Gibson, R. F. (1994). *Principles of composite material mechanics*. McGraw-Hill.
- [Goldberg, 1989] Goldberg, D. (1989). *Genetic Algorithms in Search, Optimization and Machine Learning*. Addison-Wesley.

- [Hashin and Shtrikman, 1963] Hashin, Z. and Shtrikman, S. (1963). A variational approach to the theory of elastic behavior of multiphase materials. *Journal of the Mechanics and Physics of Solids*, 11:127–140.
- [Hill, 1963] Hill, R. (1963). Elastic properties of reinforced solids - Some theoretical principles. *Journal of the Mechanics and Physics of Solids*, 11:357–372.
- [Hill, 1964] Hill, R. (1964). Theory of mechanical properties of fibre-strengthened materials: I. Elastic behaviour. *Journal of the Mechanics and Physics of Solids*, 12:199–212.
- [Hill, 1965] Hill, R. (1965). A self-consistent mechanics of composite materials. *Journal of the Mechanics and Physics of Solids*, 13:213–222.
- [Holland, 1975] Holland, J. H. (1975). *Adaptation in Natural and Artificial Systems*. MIT Press.
- [Houck et al., 1995] Houck, C. R., Joines, J. A., and Kay, M. G. (1995). A Genetic Algorithm for function Optimization: A Matlab implementation. Technical Report NCSU-IE TR 95-09, North Carolina State University. Also available as http://www.fmmcenter.ncsu.edu/fac_staff/joines/papers/gaot.ps.
- [Hudec, 1999] Hudec, B. (1999). *Programovací techniky*. ČVUT.
- [Ingber, 1993] Ingber, L. (1993). Simulated annealing: Practice versus theory. *Mathematical and Computer Modelling*, 18(11):29–57.
Also available as http://www.ingber.com/asa93_sapvt.ps.gz.
- [Ingber, 1995] Ingber, L. (1995). Adaptive simulated annealing (ASA): Lessons learned. *Control and Cybernetics*, 25(1):33–54.
Also available as http://www.ingber.com/asa96_lessons.ps.gz.

- [Kirkpatrick et al., 1983] Kirkpatrick, S., Gelatt, Jr., C., and Vecchi, M. P. (1983). Optimization by Simulated Annealing. *Science*, 220:671–680.
- [Kohler and Papanicalou, 1982] Kohler, W. and Papanicalou, G. C. (1982). Bound for the overall conductivity of random media. In Burridge, R., Childress, S., and Papanicolaou, G., editors, *Macroscopic properties of disordered media*, volume 24 of *Lecture Notes in Physics*, pages 111–130. Courant Institute, Springer-Verlag, Berlin.
- [Kvasnička, 1993] Kvasnička, V. (1993). Stochastické metody optimalizace funkcí N premenných. In *Analýza dat*, Pardubice.
- [Kvasnička, 1999] Kvasnička, V. (1999). *Evolučné algoritmy*. In preparation.
- [Mahfoud and Goldberg, 1992] Mahfoud, S. and Goldberg, D. E. (1992). A genetic algorithm for parallel simulated annealing. In Manner, R. and Manderick, B., editors, *Parallel Problem from Nature*, volume 2, pages 301–310. North-Holland, Amsterdam.
- [Markov, 1998] Markov, K. Z. (1998). On the cluster bounds for the effective properties of microcracked solids. *Journal of the Mechanics and Physics of Solids*, 46(2):357–388.
- [Michalewicz, 1992] Michalewicz, Z. (1992). *Genetic Algorithms + Data Structures = Evolution Programs*. AI Series. Springer-Verlag, New York.
- [Michalewicz et al., 1994] Michalewicz, Z., Logan, T. D., and Swaminathan, S. (1994). Evolutionary operators for continuous convex parameter spaces. In Sebald, A. and Fogel, L., editors, *Proceedings of the 3rd Annual Conference on Evolutionary Programming*, pages 84–97, River Edge, NJ. World Scientific Publishing. Also available as <ftp://ftp.uncc.edu/coe/evol/p1.ps>.
- [Michel et al., 1999] Michel, J., Moulinec, H., and Suquet, P. (1999). Effective properties of

- composite materials with periodic microstructure: A computational approach. *Computer Methods in Applied Mechanics and Engineering*, 172:109–143.
- [Milton, 1982] Milton, G. W. (1982). Bounds on the elastic and transport properties of two-component composites. *Journal of the Mechanics and Physics of Solids*, 30(3):177–191.
- [Mori and Tanaka, 1973] Mori, T. and Tanaka, K. (1973). Average stress in matrix and average elastic energy of elastic materials with misfitting inclusions. *Acta Metallurgica*, 21:571.
- [Ponte Castañeda and Willis, 1995] Ponte Castañeda, P. and Willis, J. (1995). The effect of spatial distribution on the effective behavior of composite materials and cracked media. *Journal of the Mechanics and Physics of Solids*, 43(12):1919–1951.
- [Povirk, 1995] Povirk, G. L. (1995). Incorporation of microstructural information into models of two-phase materials. *Acta metall. mater.*, 43(8):3199–3206.
- [Press et al., 1992] Press, W. H., Teukolsky, S. A., Vetterling, W. T., and Flannery, B. P. (1992). *Numerical recipes in C*. Cambridge University Press, 2nd edition. Also available as <http://www.nr.com>.
- [Pyrz, 1994] Pyrz, R. (1994). Correlation of microstructure variability and local stress field in two-phase materials. *Materials Science and Engineering*, A177:253–259.
- [Quintanilla and Torquato, 1997] Quintanilla, J. and Torquato, S. (1997). Microstructure functions for a model of statistically inhomogeneous random media. *Physical Review E*, 55(2):1558–1565.
- Also available as <http://www.cherypit.princeton.edu/papers/paper-131.pdf>.
- [Rektorys, 1995a] Rektorys, K., editor (1995a). *Přehled užité matematiky*, volume 2. Prometheus, 6th edition.

- [Rektorys, 1995b] Rektorys, K., editor (1995b). *Přehled užití matematiky*, volume 1. Prometheus, 6th edition.
- [Reuss, 1929] Reuss, A. (1929). Berechnung der fließgrenze von mischkristallen auf grund der plastizitatesbedingung für einkristalle. *Z. Ang. Math. Mech.*, 9:49.
- [Ripley, 1977] Ripley, B. (1977). Modeling of spatial patterns. *Journal of the Royal Statistical Society - Series B (methodological)*, 39(2):172–192.
- [Sejnoha, 1999] Sejnoha, M. (1999). *Micromechanical analysis of unidirectional fibrous composite plies and laminates*, volume 3 of *CTU Reports*. Czech Technical University in Prague.
- [Smith and Torquato, 1988] Smith, P. and Torquato, S. (1988). Computer simulation results for the two-point probability function of composite media. *Journal of Computational Physics*, 76:176–191.
- [Storn, 1996] Storn, R. (1996). On the usage of differential evolution for function optimization. In *NAPHIS 1996*, pages 519–523. Berkeley.
Also available as <http://www.icsi.berkeley.edu/~storn/bisc1.ps.gz>.
- [Storn and Price, 1995] Storn, R. and Price, K. (1995). Differential Evolution : A simple and efficient adaptive scheme for global optimization over continuous spaces. Technical Report TR-95-012, University of Berkeley.
Also available as <ftp://www.icsi.berkeley.edu/pub/techreports/tr-95-012.ps.gz>.
- [Suquet, 1987] Suquet, P. (1987). Elements of homogenization for inelastic solid mechanics. In Sanchez-Palencia, E. and Zaoui, A., editors, *Homogenization Techniques for Composite Media*, volume 272 of *Lecture notes in physics*, pages 194–278. Springer-Verlag, Berlin.

- [Teplý and Dvořák, 1988] Teplý, J. L. and Dvořák, G. J. (1988). Bound on overall instantaneous properties of elastic-plastic composites. *Journal of the Mechanics and Physics of Solids*, 36(1):29–58.
- [Torquato, 1991] Torquato, S. (1991). Random heterogeneous media: Microstructure and improved bound on effective properties. *Applied Mechanics Review*, 44(2):37–76.
- [Torquato and Stell, 1982] Torquato, S. and Stell, G. (1982). Microstructure of two-phase random media. I. The n -point probability functions. *Journal of Chemical Physics*, 77(4):2071–2077.
- [Torquato and Stell, 1985] Torquato, S. and Stell, G. (1985). Microstructure of two-phase random media. V. The n -point matrix probability functions for impenetrable spheres. *Journal of Chemical Physics*, 82(2):980–987.
- [Voight, 1887] Voight, W. (1887). Theoretische studien uber die elastizitatsverhaltnisse der klustalle. *Abh. Klg. Ges. Wiss. Gottingen, Math. Kl.*, 34:47.
- [Willis, 1977] Willis, J. R. (1977). Bounds and self-consistent estimates for the overall properties of anisotropic composites. *Journal of the Mechanics and Physics of Solids*, 25:185–202.
- [Yeong and Torquato, 1998] Yeong, C. L. Y. and Torquato, S. (1998). Reconstructing random media. *Physical Review E*, 57(1):495–506.
- [Yuret, 1994] Yuret, D. (1994). From genetic algorithms to efficient optimization. Technical Report 1569, Massachusetts Institute of Technology, Artificial Intelligence Laboratory. Also available as <http://www.ai.mit.edu/people/deniz/publications/aitr1569.ps.gz>.

Appendix A

EVALUATION OF $M(r)$ FOR IMPENETRABLE CYLINDERS

The function $M(r)$ appears in the relation for the two-point matrix probability function of particulate media (see Eq.(2.39)). For the statistically isotropic media, it takes the form

$$M(r_{12}) = \int \int h(r_{34})m(r_{13})m(r_{24})d\mathbf{r}_3d\mathbf{r}_4. \quad (\text{A.1})$$

To obtain this function, the two-dimensional Fourier's transform of individual members of previous equation must be found. The two-dimensional Fourier's transform is given by

$$\hat{F}(\mathbf{t}) = \int F(\mathbf{x})e^{-i\mathbf{x}\cdot\mathbf{t}}d\mathbf{x}, \quad (\text{A.2})$$

and the inverse Fourier's transform is provided by

$$F(\mathbf{x}) = \frac{1}{4\pi^2} \int \hat{F}(\mathbf{t})e^{i\mathbf{x}\cdot\mathbf{t}}d\mathbf{t}. \quad (\text{A.3})$$

Let start with the evaluation of $\hat{h}(t)$, given by

$$\hat{h}(\mathbf{t}) = \int h(\mathbf{x})e^{-i\mathbf{t}\cdot\mathbf{x}}d\mathbf{x}. \quad (\text{A.4})$$

Substitution of (A.4) into polar coordinates leads to

$$\begin{aligned} \hat{h}(t, \theta) &= \int_0^\infty \int_0^{2\pi} h(r)e^{-irt(\cos\theta\cos\phi+\sin\theta\sin\phi)}r\,drd\phi = \\ &= \int_0^\infty \int_0^{2\pi} h(r)e^{-irt(\sin(\theta-\phi))}r\,drd\phi = \\ &= \int_0^\infty h(r)r\left(\int_0^{2\pi} e^{-irt\sin\alpha}d\alpha\right)dr \end{aligned} \quad (\text{A.5})$$

Noticing, that bracketed term can be rewritten as (see eg. [Rektorys, 1995b, p. 663])

$$\int_0^{2\pi} e^{-irt\sin\alpha}d\alpha = 2\pi J_0(rt), \quad (\text{A.6})$$

where J_0 is the Bessel's function of the first kind and 0-th order, we arrive at expression

$$\boxed{\hat{h}(t) = 2\pi \int_0^\infty h(t) J_0(rt) r \, dr}. \quad (\text{A.7})$$

Furthermore, integral (A.7) can be determined using the function $K(r)$ instead of $h(r)$. Recall how the function $g_2(r)$ is derived from $K(r)$ (Eq. (2.32)) and proceed in similar fashion. Thus,

$$\begin{aligned} \hat{h}(t) &= 2\pi \int_0^\infty h(r) r J_0(rt) \, dr = 2\pi \int_0^\infty \frac{1}{2\pi r} \frac{d\tilde{K}(r)}{dr} r J_0(rt) \, dr = \\ &= \int_0^\infty \frac{d\tilde{K}(r)}{dr} J_0(rt) \, dr = \boxed{t \int_0^\infty \tilde{K}(r) J_1(rt) \, dr} + \left[J_0(rt) \tilde{K}(r) \right]_0^\infty, \end{aligned} \quad (\text{A.8})$$

where the function $\tilde{K}(r) = K(r) - \pi r^2$ is a counterpart of the function $h(r)$ and J_1 is the Bessel's function of the first kind and first order. The last term in Eq. (A.8) vanishes, because $\tilde{K}(0) = 0$ and for $r \rightarrow \infty$ $J_0(rt) \rightarrow 0$ and $K(r) \rightarrow \text{const.}$

The value of $\widehat{m}(t)$ is provided by

$$\widehat{m}(t) = 2\pi \int_0^\infty H(R-r) J_0(rt) r \, dr = 2\pi \int_0^R J_0(rt) r \, dr. \quad (\text{A.9})$$

Note that (see [Rektorys, 1995b, p. 664])

$$\frac{d}{dr}(r J_1(r)) = J_1(r) + r \frac{dJ_1(r)}{dr} = J_1(r) + (-J_1(r) + r J_0(r)) = r J_0(r),$$

so integral (A.9) yields

$$\widehat{m}(t) = \left[\frac{2\pi r}{t} J_1(rt) \right]_0^R = \boxed{\frac{2\pi R}{t} J_1(Rt)} \quad (\text{A.10})$$

Using similar procedure and employing the relation (A.7), the inverse transform of function $\widehat{M}(t)$ can be obtained as

$$M(r) = \frac{1}{2\pi} \int_0^\infty \widehat{M}(t) t J_0(rt) \, dt. \quad (\text{A.11})$$

Appendix B

PARAMETER SETTINGS FOR OPTIMIZATION ALGORITHMS

<i>Algorithm</i>	<i>Parameters</i>	<i>Value</i>	<i>Description</i>
POWELL	Step_init	R	Initial step length
DHC	Step_init	R	Initial step length
	Step_min	0.001	Minimum step length
BFGS	ε	10^{-2}	Step for numerical differentiation

Table B.1: Deterministic algorithms parameters

<i>Parameters</i>	<i>Value</i>	<i>Description</i>
N_pop	64	Size of population
b	2	Shape parameter for non-uniform mutation
C_mult	2.	Ratio of maximum/average scaled fitness
N_mut_crs	2	Ratio of mutation/crossover operators
N_heu_max	10	Maximum number of heuristic crossovers in one cycle

Table B.2: Parameter settings for **GA I**

<i>Parameters</i>	<i>Value</i>	<i>Description</i>
N_pop	64	Size of population
b	2.	Shape parameter for non-uniform mutation
C_mult	1.2	Ratio of maximum/average scaled fitness
N_heu_max	10	Maximum number of heuristic crossovers in one cycle
N_uni_mut	8	Number of uniform mutations for one generation
N_bnd_mut	8	Number of boundary mutations for one generation
N_nun_mut	8	Number of non-uniform mutations for one generation
N_mnu_mut	8	Number of multi-non-uniform mutations for one generation
N_smp_crs	4	Number of simple crossover for one generation
N_sar_crs	4	Number of simple arithmetic crossover for one generation
N_war_crs	4	Number of whole arithmetic crossover for one generation
N_heu_crs	4	Number of heuristic crossovers for one generation

Table B.3: Parameter settings for **GA II**

<i>Parameters</i>	<i>Value</i>	<i>Description</i>
N_pop	8	Size of population
N_pop_det	4	Number of individuals used for DHC
N_pop_max	20	Number of populations before application of DHC
N_heu_max	10	Maximum number of heuristic crossovers in one cycle
N_smp_crs	1	Number of simple crossover for one generation
N_sar_crs	1	Number of simple arithmetic crossover for one generation
N_war_crs	1	Number of whole arithmetic crossover for one generation
N_heu_crs	1	Number of heuristic crossovers for one generation

Table B.4: Parameter settings for **HGA**

<i>Parameters</i>	<i>Value</i>	<i>Description</i>
N_pop	64	Size of population
b	2.	Shape parameter for non-uniform mutation
C_mult	1.2	Ratio of maximum/average scaled fitness
N_heu_max	10	Maximum number of heuristic crossovers in one cycle
N_uni_mut	3	Number of uniform mutations for one generation
N_bnd_mut	3	Number of boundary mutations for one generation
N_nun_mut	3	Number of non-uniform mutations for one generation
N_mnu_mut	3	Number of multi-non-uniform mutations for one generation
N_smp_crs	1	Number of simple crossover for one generation
N_sar_crs	1	Number of simple arithmetic crossover for one generation
N_war_crs	1	Number of whole arithmetic crossover for one generation
N_heu_crs	1	Number of heuristic crossover for one generation

Table B.5: Parameter settings for **GA III**

<i>Parameters</i>	<i>Value</i>	<i>Description</i>
N_pop	200	Size of population
F	.6	
CR	.9	Crossover rate

Table B.6: Parameter settings for **DE**

<i>Parameters</i>	<i>Value</i>	<i>Description</i>
N_pop	64	Size of population
q	.08	Probability of selecting best individual
b	2.	Shape parameter for non-uniform mutation
N_heu_max	10	Maximum number of heuristic crossovers in one cycle
p_uni_mut	.225	Probability of uniform mutation
p_bnd_mut	.225	Probability of boundary mutation
p_nun_mut	.225	Probability of non-uniform mutation
p_mnu_mut	.225	Probability of multi-non-uniform mutation
p_smp_crs	.025	Probability of simple crossover
p_sar_crs	.025	Probability of simple arithmetic crossover
p_war_crs	.025	Probability of whole arithmetic crossover
p_heu_crs	.025	Probability of heuristic crossover
T_max	.1	Ratio of T_max and average F of starting population
T_min	$\varepsilon/10$	Minimum temperature
T_mult	.9	Ration of cooling
N_success_max	500	Maximum number of accepted individuals
N_counter_max	5000	Maximum number of iteration for fixed T

Table B.7: Parameter settings for **AUSA**

<i>Parameters</i>	<i>Value</i>	<i>Description</i>
W	1500	Length of adaptation window
I	1000	Adaptation interval
M	10	Generations to be considered back
P	.9	Proportion of Δ to pass back

Table B.8: Adaptivity parameters setting

<i>Parameters</i>	<i>Value</i>	<i>Description</i>
N_pop	64	Size of population
q	.08	Probability of selecting best individual
b	2.	Shape parameter for non-uniform mutation
N_heu_max	10	Maximum number of heuristic crossovers in one cycle
p_uni_mut	.3	Probability of uniform mutation
p_nun_mut	.3	Probability of non-uniform mutation
p_mnu_mut	.3	Probability of multi-non-uniform mutation
p_s2p_crs	.1	Probability of two-point crossover
T_max	.1	Ratio of T_max and average F of starting population
T_min	$\varepsilon/10$	Minimum temperature
T_mult	.9	Ration of cooling
N_success_max	500	Maximum number of accepted individuals
N_counter_max	5000	Maximum number of iteration for fixed T

Table B.9: Parameter settings for **AUSA** with problem-dependent operators